CRREL REPORT 82-24

4222

US Army Corps of Engineers
Cold Regions Research & Engineering Laboratory

Subsea permafrost in Harrison Bay, Alaska

An interpretation from seismic data

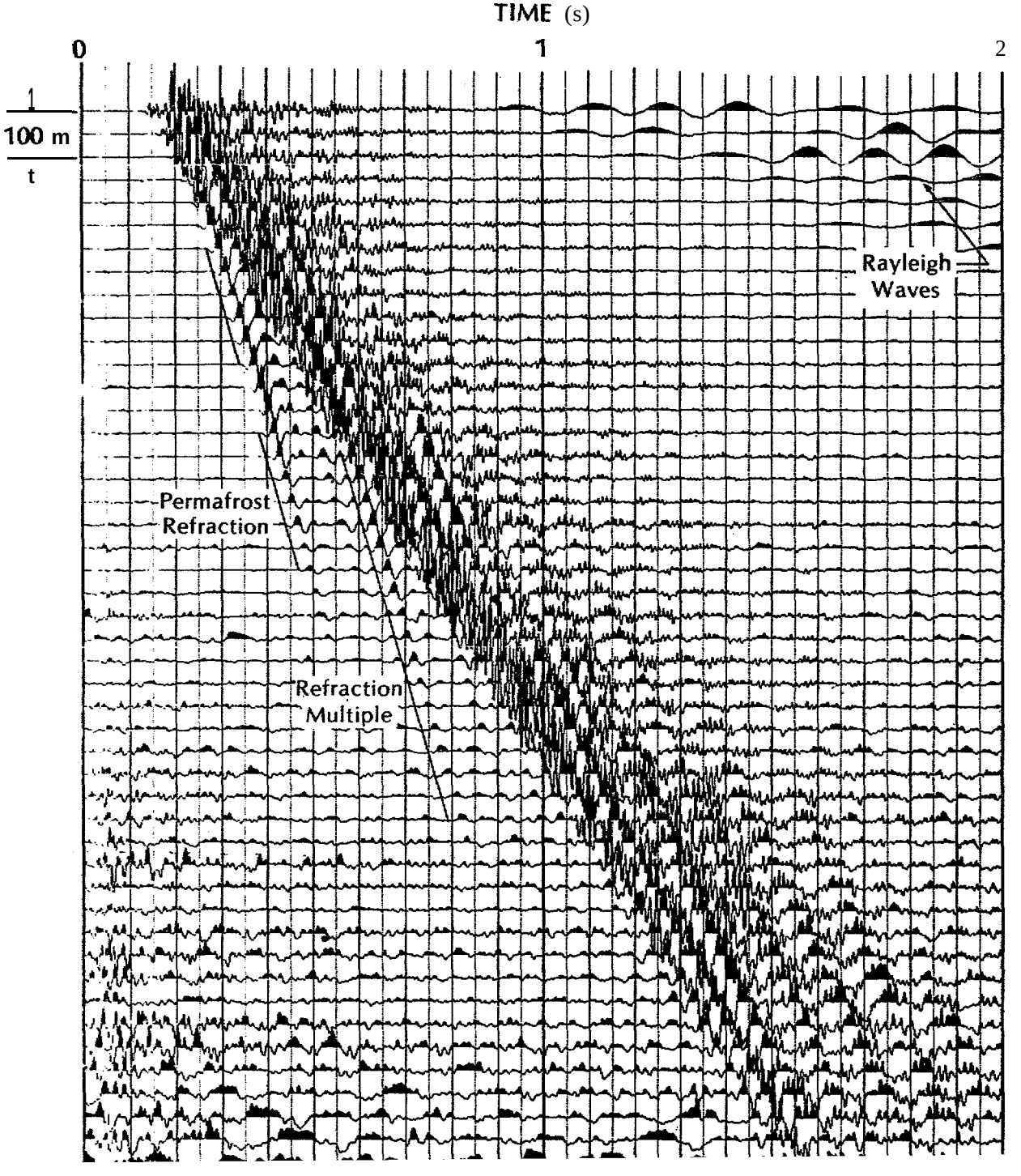

Cover: Sample marine record showing high-velocity refractors interpreted as sub-sea permafrost.

CRREL Report 82-24

August 1982

Subsea permafrost in Harrison Bay, Alaska

An interpretation from seismic data

K. Gerard Neave and Paul V. Sellmann

Prepared for
BUREAU OF LAND MANAGEMENT **and**
NATIONAL OCEANIC AND ATMOSPHERIC ADMINISTRATION

REPORT DOCUMENTATION PAGE

READ INSTRUCTIONS BEFORE COMPLETING FORM

REPORT NUMBER: CRREL Report 82-24

2. GOVT ACCESSION NO.

3. RECIPIENT'S CATALOG NUMBER

TITLE (and Subtitle)

SUBSEA PERMAFROST IN HARRISON BAY, ALASKA: AN INTERPRETATION FROM SEISMIC DATA

5. TYPE OF REPORT & PERIOD COVERED

6. PERFORMING ORG. REPORT NUMBER

7. AUTHOR(s)

K. Gerard Neave and Paul V. Sellmann

8. CONTRACT OR GRANT NUMBER(E)

Contract no. 01-5-022-2313

PERFORMING ORGANIZATION NAME AND ADDRESS

U.S. Army Cold Regions Research and Engineering Laboratory
72 Lyme Road
Hanover, New Hampshire 03755

10. PROGRAM ELEMENT, PROJECT, TASK AREA & WORK UNIT NUMBERS

CONTROLLING OFFICE NAME AND ADDRESS

Dept. of Interior, Bureau of Land Management, Washington, D.C. and Dept. of Commerce, National Oceanic and Atmospheric Administration/ RL, Boulder, Colorado

12. REPORT DATE

August 1982

13. NUMBER OF PAGES

65

14. MONITORING AGENCY NAME & ADDRESS (If different from Controlling Office)

15. SECURITY CLASS. (of this report)

Unclassified

15a. DECLASSIFICATI ON/DOWNGRADING SCHEDULE

16. DISTRIBUTION STATEMENT (of this Report)

Approved for public release; distribution unlimited

17. DISTRIBUTION STATEMENT (of the abstract entered in Block 20, If different from Report)

18. SUPPLEMENTARY NOTES

19. KEY WORDS (Continue on reverse side if necessary and identify by block number)

Alaska-Seismology
Beaufort Sea-seismology
Permafrost
Seismic data
Seismic detection
Seismic reflection
Seismic signatures
Seismology

20. ABSTRACT (Continue on reverse side if necessary and identify by block number)

Velocity data derived from petroleum industry seismic records from Harrison Bay show that high-velocity material (> 2 km/s) interpreted to be ice-bonded permafrost is common; In the eastern part of the bay, the depth to high velocity material increases and velocity decreases in an orderly manner with increasing distance from shore until the layer is no longer apparent. The western part of the bay is less orderly, possibly reflecting a different geological and thermal history. This western part may bean inundated section of the low coastal plain characterized by the region north of Teshekpuk Lake, and could have contained deep thaw lakes, creating low velocity zones. Along some seismic lines, the high-velocity material extends approximately 25 km offshore.

20. Abstract (cent'd).

Two anomalies have been found which could be associated with rapidly degrading permafrost. One is strong attenuation, which was interpreted as an indication of gas in the shallow deposits. The other is the presence of considerable seismic noise, including identifiable small seismic events. The origin of this noise has not been positively established, and it is proposed that it may indicate that some movement is occurring in the sediments due to thaw.

PREFACE

This report was prepared by Dr. K. Gerard Neave, Consultant Geophysicist, and Paul V. Sellmann, Geologist, Geotechnical Research Branch, Experimental Engineering Division, U.S. Army Cold Regions Research and Engineering Laboratory. Funding *was* provided wholly by the Bureau of Land Management through an interagency agreement with the National Oceanic and Atmospheric Administration, as part of the Outer Continental Shelf Environmental Assessment Program. This report was prepared as part of CRREL'S study of the distribution of subsea permafrost in the Alaskan Beaufort Sea.

The geophysical data used for this study were acquired from Western Geophysical Company of America and from British Petroleum, Alaska, Inc. The authors greatly appreciate the cooperation received from these companies. They also gratefully acknowledge the helpful suggestions and constructive comments made by the reviewers of this report, Dr. Steven Arcone and Donald Albert of CRREL.

CONTENTS

ILLUSTRATIONS

Figure

TABLES

Table

SUBSEA PERMAFROST IN HARRISON BAY, ALASKA
An Interpretation from Seismic Data

K. Gerard Neave and Paul V. Sellmann

INTRODUCTION

The objective of this study was to obtain information, through analysis of seismic records, on the distribution and properties of subsea permafrost in the Harrison Bay region of the Alaskan Beaufort Sea.

Information on this region is based primarily on seismic studies. No core drilling or sample analysis has been done, although temperature data and observations of penetration resistance have been obtained from shallow probe observations (Harrison and Osterkamp 1981). Several high-resolution seismic lines were run by Rogers and Morack (1981). However, the penetration achieved during their study (40 m) largely precluded the detection of deeper high-velocity material. The lack of deeper drilling and core analysis has resulted in a critical deficiency in ground truth data to verify the seismic interpretation.

This investigation is based on the interpretation of monitor seismic records from petroleum exploration programs. The first-return data used included speculative and nonproprietary data from Western Geophysical Company of America, plus data released by British Petroleum. A total of approximately 450 km of seismic line, with one record per kilometer, was examined. The locations of these lines are shown in Figure 1.

The data for shoreline transitions and other shallow water coastal areas are from a winter survey conducted over the ice. The remaining shot lines are from a marine survey. A summary of the field parameters used in collecting both sets of data is presented in Table 1.

In seismic data processing for petroleum exploration the emphasis is normally on deep targets, commonly with first-break suppression, increased gain with time, time-variable fibers, and normal move-out corrections. These procedures tend to compromise the quality of the data from near the surface. To obtain as much information as possible from the records without costly processing, monitor records were produced by playing back approximately the first 2 seconds of the field tapes with expanded gain. They were printed in a "wiggletrace" or variable area format, without normal move-out corrections, or filtering.

An appreciable increase in seismic velocity occurs when most unconsolidated materials freeze (Aptikaev 1964). This increase, and the existence of large amounts of seismic data from surveys conducted for petroleum exploration, make seismic techniques a reasonable approach for investigating the distribution of ice-bonded subsea permafrost. Hunter et al. (1976) and Sellmann et al. (1980) have shown that when records are available, and their quality and field recording parameters are appropriate, permafrost data can be extracted from the monitor records. Direct wave velocities and refraction interpretation of the first returns can give information on velocity structure (Fig. 2). These velocity data are used to predict the distribution of ice-bonded permafrost and, when resolution is adequate, the depth to the top of the frozen sediments. Reflection interpretations also supplement the depth information when shallow reflectors are strong enough.

A number of error estimates are presented in the *Spatial Resolution* section to verify that the measurements and analytical methods are reasonable. These estimates are not intended to set strict limits

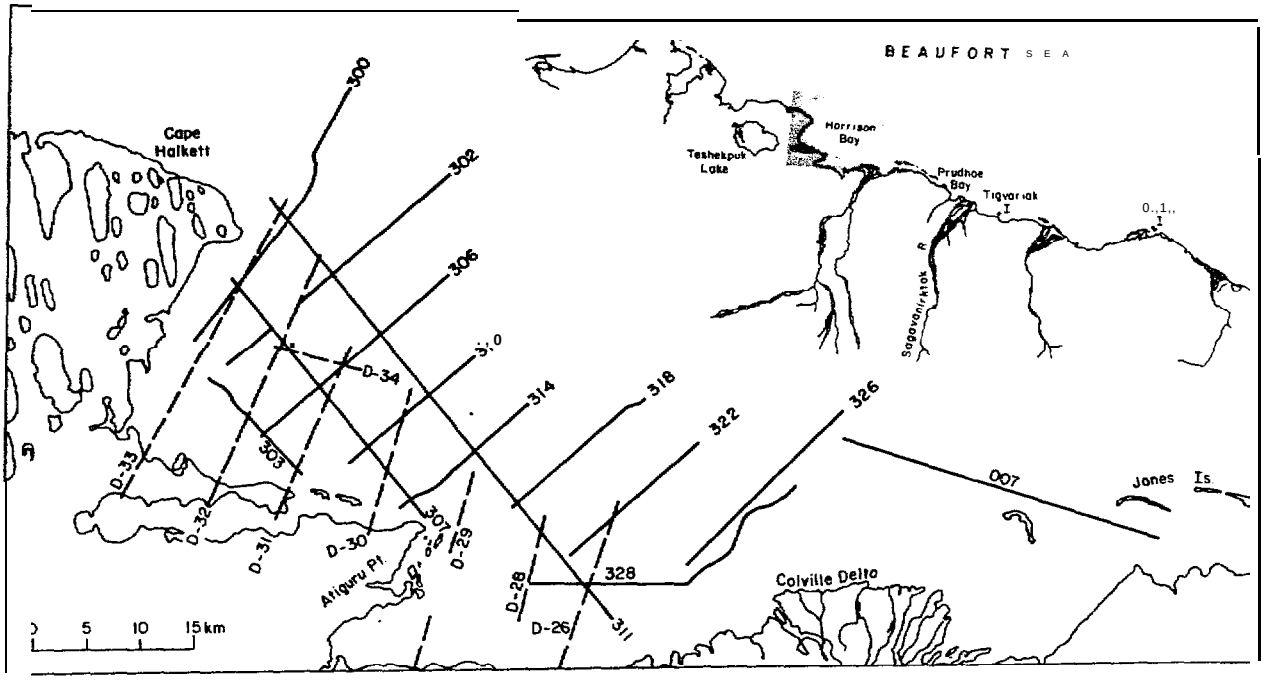

Figure 1. Harrison Bay area. Solid lines are from a marine survey and dashed lines from an ice survey.

Table 1. **Harrison Bay survey specifications.**

	BP Alaska ice survey	*Western Geophysical shallow water marine*
Source	Explosives (23 kg or 50 lb)	10 air guns, 9500 cm' (580 in'.), each at a pressure of 21,000 kPa (3000 psi)
Distance from center of source to center of nearest receiver group	50 m	278 or 256 m
Receiver array	48 groups split spread	4S groups bottom drag cable
Group interval	100 m	50 m or 30.5 m
Recording method	digital	digital
Sampling rate	2 ms	2 ms
Low fibers	8 Hz	5.3 Hz
High filters	124 Hz	128 Hz

on interpretation error, since difficulties in seismic data acquisition and analysis may occur which cannot be evaluated. For example, signal identification is occasionally a problem. Late-arriving reflections can be misinterpreted as refraction events, particularly when the signal-to-noise level is low. Another problem can be created by the need to assume plane layers for simplicity in interpretation, whereas localized curvature of reflecting and refracting surfaces can be expected due to roughness on the upper surface of degrading subsea permafrost. Both of these problems are deah with primarily by looking at the internal consistency of the results where there is duplication in coverage, and finally by verification with independent geophysical techniques and drilling results.

In addition to the refraction and reflection interpretations, two seismic anomalies were mapped that appear to be directly related to degrading permafrost. Anomalous attenuation rates were observed and natural noise sources were found in some areas. The occurrence of these anomalies in

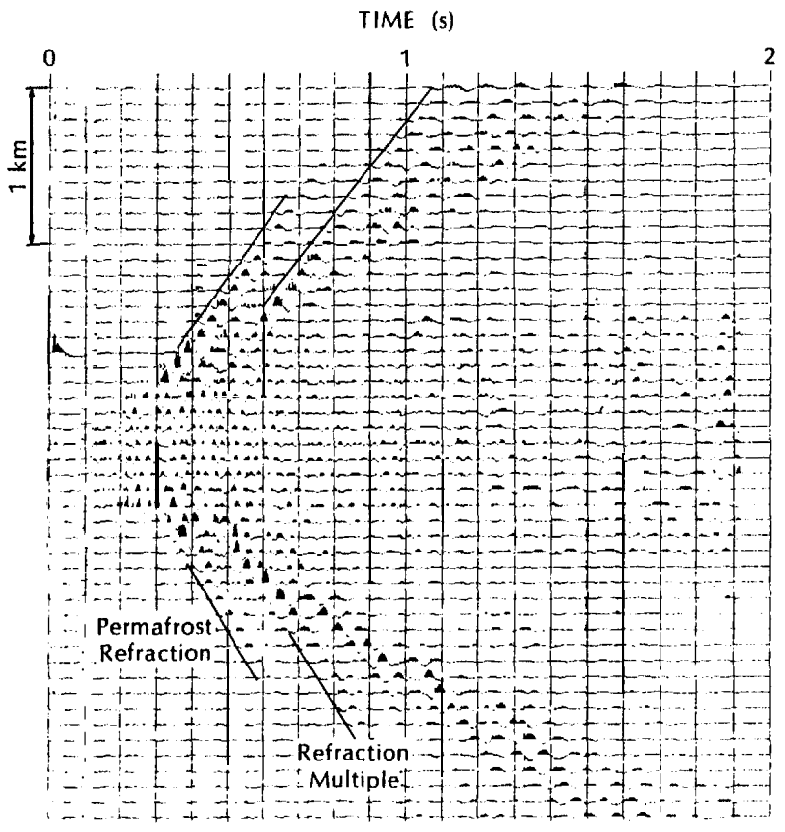

a. An ice shooting record with refractor velocities of 3.1 and 3.5 km/s for the upper and lower spreads, respectively. A refraction multiple can be seen on both spreads.

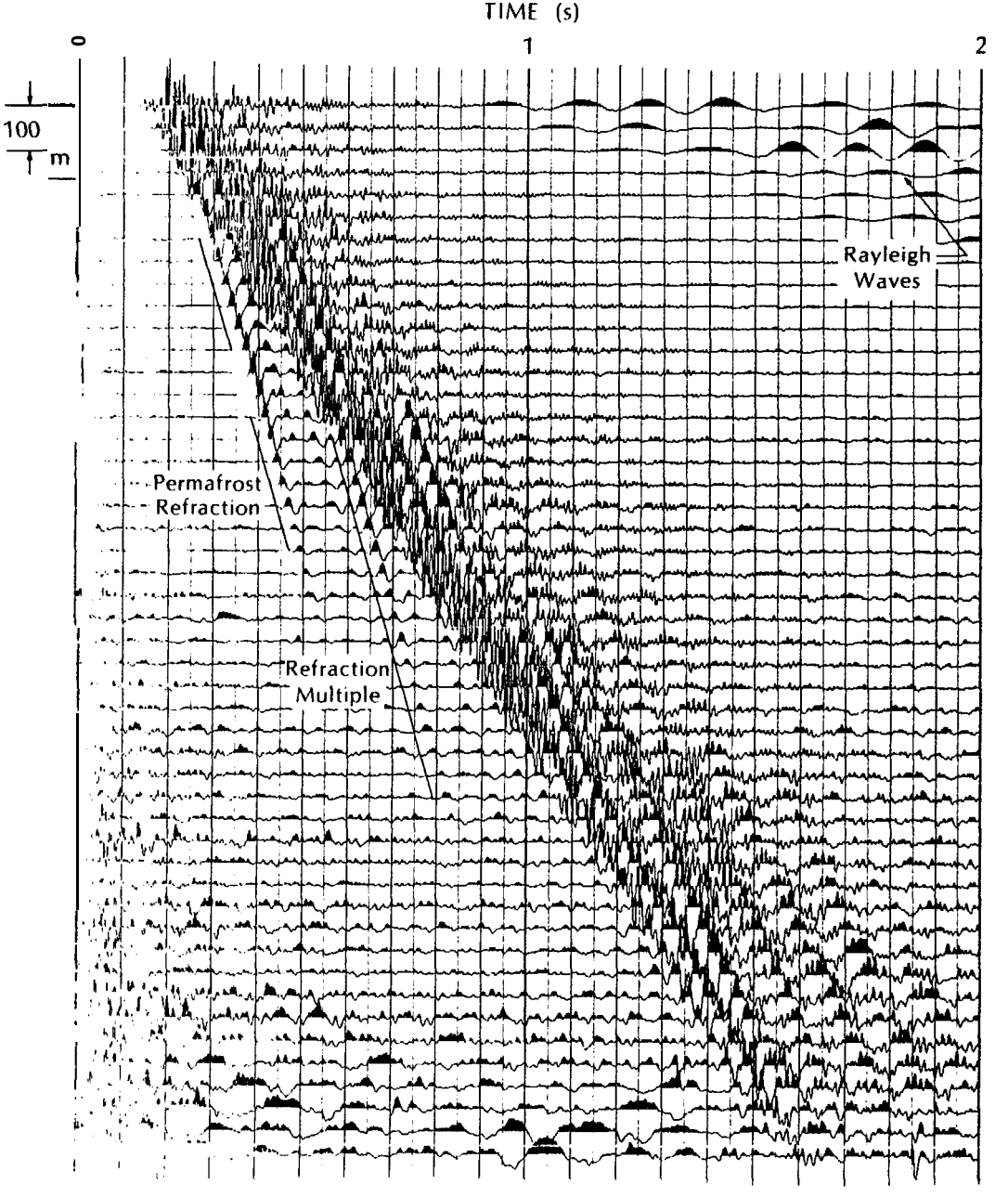

b. A marine record with refractor velocities of 3.3 and 3.8 km/s. A strong refraction multiple is also present, plus low frequency, low velocity Rayleigh waves.

Figure 2. Sample monitor records showing high-velocity refractors interpreted as subsea permafrost.

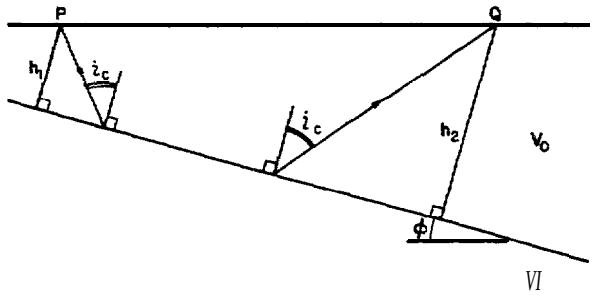

Figure 3. Ray path geometry for Q refractor dipping at an angle φ. The shot is at P and the receiver is at Q for the down-dip shot. The shot and receiver positions are reversed for the up-dip shot.

relation to distribution of permafrost is discussed in the text.

The process of attenuation involves the absorption of *a* percentage of the transmitted energy with each cycle of the wave propagation. Since high frequencies have shorter wavelengths relative to low frequencies, one can usually perceive attenuation as low pass filtering or pulse broadening of the signal. Small attenuation losses are usually observed in saturated marine sediments (Winkler and Nur 1979). However, drastic attenuat ion cart be expected when a liquid and gas are combined in the sediment pores.

Failure of materials due to deformation can cause small-scale seismic events. Some movement and differential settlement can be expected in the Harrison Bay sediments, and in subsea permafrost in general, as permafrost thaws in the warmer marine environment. Local induced seismicity has been observed in other regions associated with withdrawal of groundwater and extraction of fluid from petroleum reservoirs (Yerkes and Castle 1976). Thaw of pore ice in permafrost can also have the effect of reducing the pore water pressure, creating a situation analogous to fluid extraction. Localized seismic events often follow dynamite blasts in permafrost, most likely arising from release of stress developed during seasonal cooling of frozen ice-rich sediments and from volume increases due to ground ice formation. Minor earthquake activity has also been reported in the Beaufort Sea near Barter Island (Barnes and Hopkins 1978).

METHODS

Reading records

A technique for reading oil-industry monitor records has been developed for carrying out subsea permafrost surveys. The technique was originally developed for measuring velocities directly from monitor records with a drafting arm. It has now been adapted for use with a digitizing tablet for a small computer.

Three types of waves have been identified on the records and used in the analysis: refractions, reflect ions and surface waves. The same reading procedure is used for all three wave types. Each reading consists of the coordinates (x and t) for the tangent point on the time-distance plot plus a slope measurement ($c = dx/dt$) of a tangent to the curve. This information is converted to velocity data and depth profiles by means of the appropriate equations described below.

Refractions

A dipping plane layer refraction interpretation could be used on the reversed ice shooting records. Following the derivation given by Grant and West (1965) and using the geometry shown in Figure 3, the critical angle is given by $i_c = \sin^{-1}(V_0/V_1)$ where V_0 is the upper layer velocity and V_1 is the lower layer velocity. The apparent velocity" in the lower layer when shooting down-dip is

$$c^- = V_0/\sin(i_c + \phi) = V_0/\sin[\sin^{-1}(V_0/V_1) + \phi] \quad (1)$$

where ϕ is the dip of the boundary. For shooting up-dip, the apparent velocity is

$$c^+ = V_0/\sin(i_c - \phi) = V_0/\sin[\sin^{-1}(V_0/V_1) - \phi]. \quad (2)$$

Equations 1 and 2 can be combined to give an expression for the true velocity (VI) in the lower layer:

$$1/c^- + 1/c^+ = \sin(i_c + \phi)/V_0 + \sin(i_c - \phi)/V_1$$

$$= 2\sin i_c \cos\phi/V_0$$

$$= 2\cos\phi/V_1.$$

For small dip angles,

$$1/v_1 = \tfrac{1}{2}(1/c^- + 1/c^+). \quad (3)$$

Grant and West show that the distance h_1 from the up-dip shot point to the high-velocity refractor, is

$$h_1 = (V_0 t_0/2)[1 - (V_0/V_1)^2]^{-1/2} \quad (4)$$

where t_0 is the intercept time on the record. We did not measure the intercept time, but it can be easily calculated from the tangent readings. This converts eq 4 to

$$h_1 = (V_0/2)(t^- - x^-/c^-)[1 - (V_0/V_1)^2]^{-1/2}. \quad (5)$$

For purposes of constructing seismic cross sections, the depths were plotted under the midpoints of the reversed spread. An average depth ($\bar{h}$) was calculated for an array based on values from its ends:

$$\bar{h} = (V_0/4)(t^- + t^{+-} x^-/c^{--} x^+/c^+) [1 - (V_0/V_1)^2]^{-1/2}. \quad (6)$$

Equations 3 and 6 are the required equations for making velocity and depth profiles for the ice-shooting data.

There are no reversed profiles for the marine survey data; therefore, they were interpreted assuming plane horizontal layers. Equations 2 and 5 can be rewritten for horizontal layers by setting $\phi = 0$ and $c^- = c^+$:

$$V_1 = c \quad (7)$$

$$h = (V_0/2)(t - x/c)[1 - (V_0/V_1)^2]. \quad (8)$$

These two equations allow the conversion of tangent readings from the marine records to velocity and depth profiles along the marine lines.

Reflections

Reflection data analysis was based on assuming a plane horizontal reflector at a depth h under a uniform upper layer with velocity V. This simple model results in the equation of a hyperbola for the travel time t and the distance x from the shot point to the receiver (see Grant and West 1965):

$$V_0^2 t^2 = x^2 + 4h^2. \quad (9)$$

Taking differentials on both sides of the above equation gives an expression for the upper layer velocity:

$$2V_0^2 t\,dt = 2x\,dx. \quad (10)$$

Since $dx/dt = c$, eq 10 can be arranged to give the velocity in terms of the tangent readings:

$$V^* = (cX/t)^{1/2}. \quad (11)$$

Combining eq 9 and 11 gives an expression for the depth to the reflector:

$$h = (x/2)(ct/x - 1)^{1/2}. \quad (12)$$

Any tangent to a reflection curve can be converted using eq 11 and 12 into a depth and velocity determination for profile construction along the shot lines. Where possible, a number of tangents were read on each reflector, so that scatter on the plotted reflecting horizons could help to indicate the accuracy of the determinations.

Rayleigh waves

Based on the surface wave or Rayleigh wave tangent measurements, profiles were made of the phase velocity along the survey lines. These profiles proved to be useful for identifying the signals from the small quakes or noise bursts on the records.

Spatial resolution

The spatial resolution of the data from this type of study is obviously not as great as can be obtained from a seismic investigation specifically designed to study offshore permafrost. For refraction and reflection measurements, *a* number of factors must be considered, including geophone spacing, signal frequency, and complexity of the subsurface. In general, the horizontal extent of a feature that can be detected should be a minimum of three detector spacings. This means that the minimum size of a target that can be resolved is around 300 m for the ice-shooting data, and around 150 m for the marine survey data. The minimum vertical thickness of a detectable high-velocity layer is determined by the wavelength of the refracted signal (Sherwood 1967). Resolution is possible to approximately ½ wavelength or about 50 m for these data. In addition, Sherwood's results show that thin layers (less than 30 m thick) might be observed at shallow depths, but the signals from these would be in the form of plate waves at a reduced velocity and amplitude.

A simplifying assumption was used for the refraction depth determinations. The upper layer velocity was taken *as* 1.8 km/s for all profiles. This means that the water layer, O to 16 m deep, was combined with the low-velocity bottom sediments to make a single upper layer. Upper-layer velocities were observed to range from 1.6 to 2.0 km/s. Therefore, the error introduced by assuming 1.8 km/s could be as much as 30% under rare circumstances (see Appendix A).

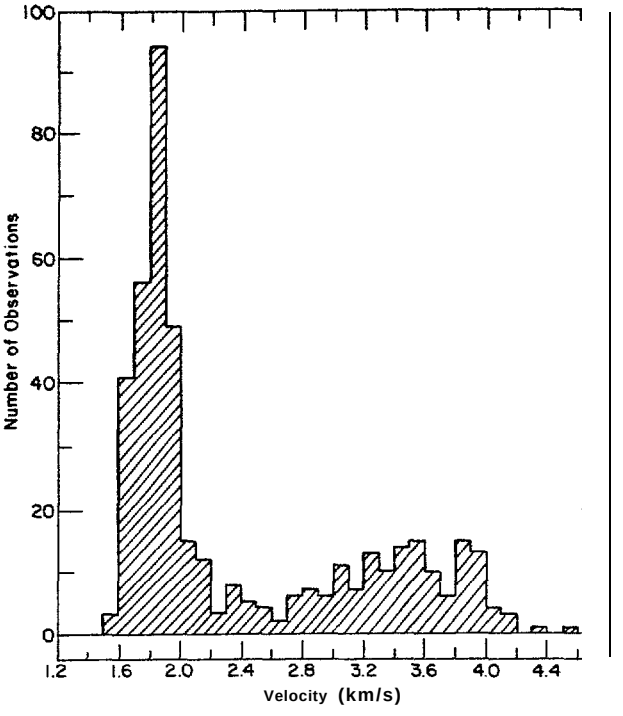

Figure 4. Velocity data from refraction analysis of Harrison Bay records.

Refraction velocities and depth determinations from single-ended marine records are subject to errors caused by dipping layers. Our interpretations indicate that dips are normally less than 3070. The corresponding maximum error is approximately 5 % in velocity measurements and 2070 in depth determinations (see Appendix A).

The assumption of horizontal layers for the reflection interpretation does not result in significant errors. Error calculat ions in Appendix A show that a 3070 dip usually results in a 1 % error in velocity and *2070* in depth.

Anomalies

Examples of the anomalous features observed on the records are shown in the text, with their distribution indicated by anomaly maps. The attenuation map was based on a simple qualitative procedure. The records examined normally have a peak frequency of 30 to 40 Hz. All records with peak frequencies lower than 15 Hz were classed as having been subject to considerable natural filtering and were grouped in the attenuation zones.

No formal attempt was made to determine the attenuation coefficients for comparison with existing data on marine sediments. Such a procedure would require spectral analysis to establish relative amplitudes at the different frequencies. This was not possible with the available records and equipment.

Examples of natural seismicit y are presented, and an anomaly map indicating the distribution was prepared for comparison with other maps including the distribution of high-velocity material and attenuation anomaly distribution. Comparative profiles were constructed of phase velocities from the natural seismicity and phase velocities from surface *waves* generated by the air guns. This velocity comparison was helpful for wave identification.

RESULTS AND DISCUSSION

Seismic velocity distribution

The range of seismic velocities observed in the Harrison Bay region is shown in Figure 4. The low velocity peak is in the range usually associated with thawed material, and the higher velocities (>2.0 km/s) are usually considered representative of chemically bonded or ice-indurated material.

The cross sections in Figures 5 and 6 represent the two velocity regimes found in Harrison Bay. Both lines have a high-velocity structure extending approximately 25 km offshore. The eastern line (Fig. 5) shows a systematic thickening of the first layer (low-velocity layer) with increasing distance from shore. The mean velocity of this upper layer (1.8 km/s) falls in the range that represents little or no ice-bonding of the sediments. The second-layer velocities of 3 to 4 km/s are consistent with ice-bonded material. In addition, the deeper layer shows a velocity decrease with depth (Fig. 5b), suggesting that the materials become warmer with depth. This thickening of the low-velocity layer with increasing distance from shore and the decrease in velocity of the second layer with depth support a model of degrading ice-bonded permafrost in an area of active marine transgression. The depth of the lower layer is greater than the depth of a similar layer observed near Prudhoe Bay, which indicates differing geological and permafrost conditions in the two regions.

The second set of profiles (Fig. 6) illustrates the greater complexity encountered in the western half of Harrison Bay. Four separate velocity zones are encountered along this line. The first segment, including the onshore records and several offshore records, is anomalous because of the low average velocities between the surface and the deep reflectors. A second segment near the shore has a shallow, high-velocity refractor. The remaining offshore half of the line has two distinct zones, one deep and one shallow, that may be partially bonded or may represent a change in material type.

The deep reflections at the south end of the line

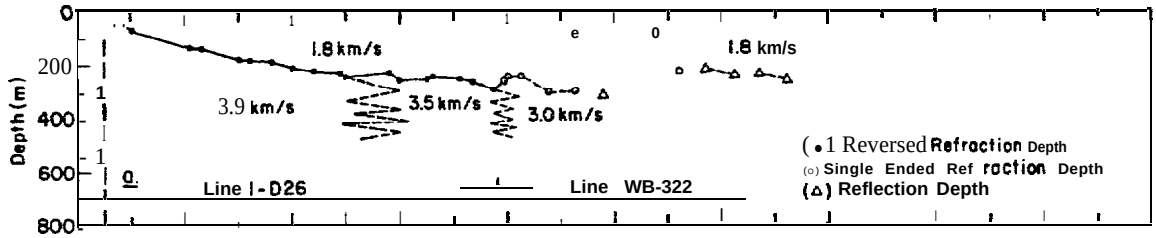

a. Cross section.

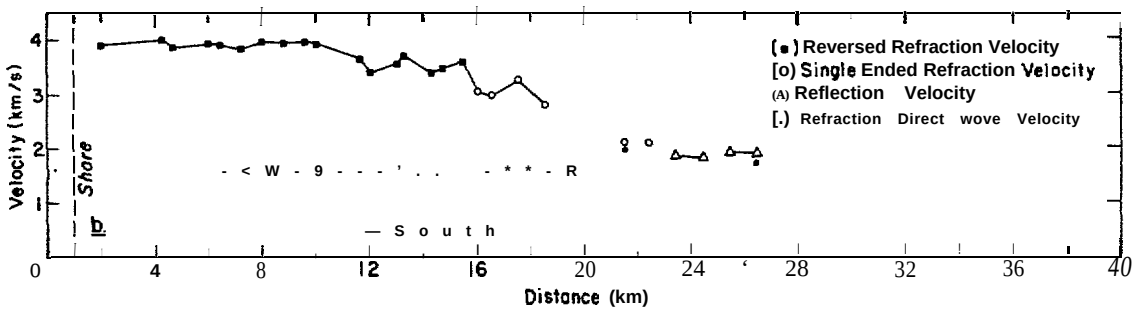

b. Velocity profile.

Figure 5. Profiles from the eastern part of Harrison Bay.

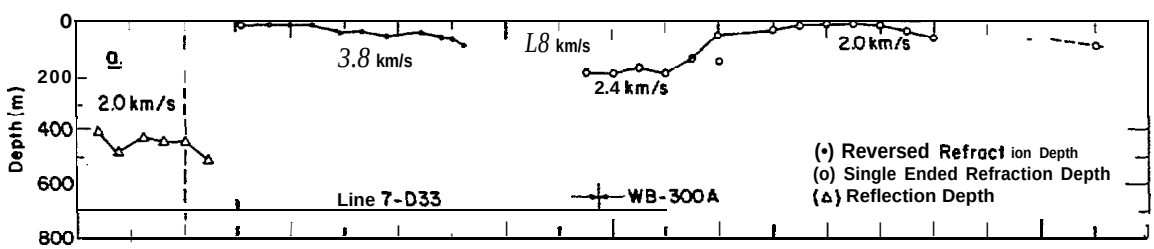

a. Cross section.

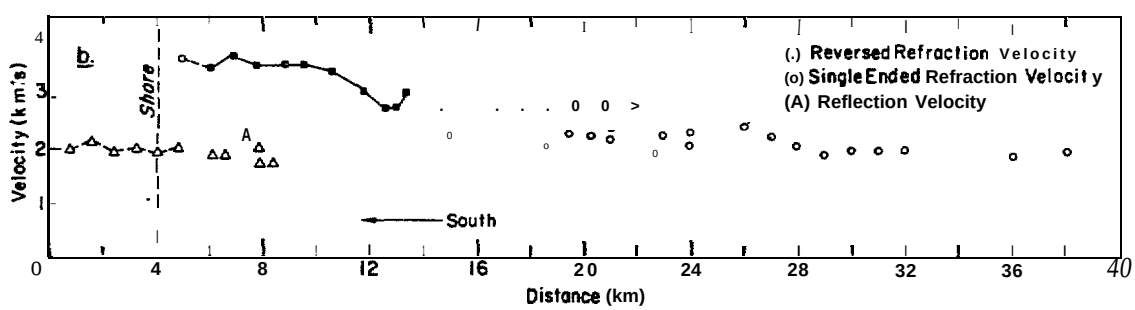

b. Velocity profile.

Figure 6. Profile from the western part of Harrison Bay.

(Fig. 6), and also on line D32 (see Appendix C), are surprising because there is only a thin layer of high-velocity material at the surface. Under that lies a thick section with low average velocity. The low-velocity zone could be explained as a thaw zone formed beneath a lake that historically occupied the surface in this area. This would imply that recent near-surface temperatures are low due to exposure of the surface as a result of draining of the thaw lake basin. The deeper sediments down to 400 m are warmer, reflecting the previous warming cycle induced by the lake environment. The low velocities could also be explained by a contrast in material properties. If the thin surface

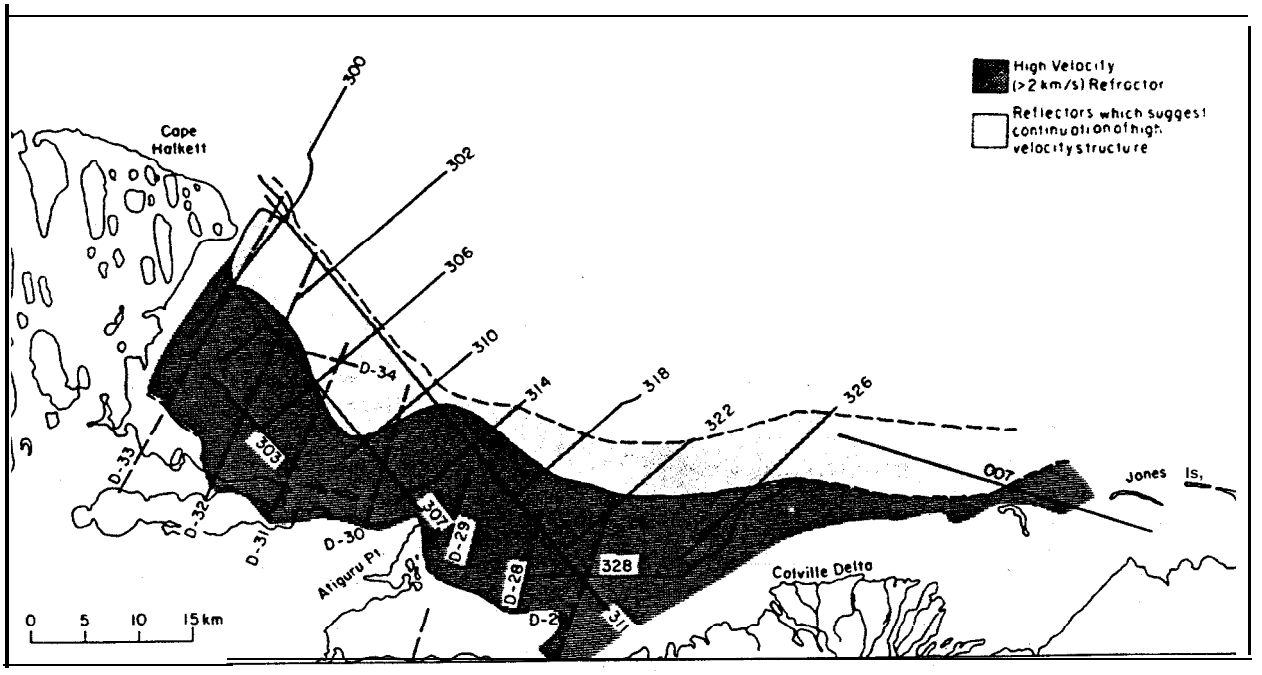

Figure 7. Distribution of high-velocity material in Harrison Bay. A continuous high velocity is present between the shore and the first contour line. Reflection readings show that this feature can be followed farther offshore to the second contour line before it disappears.

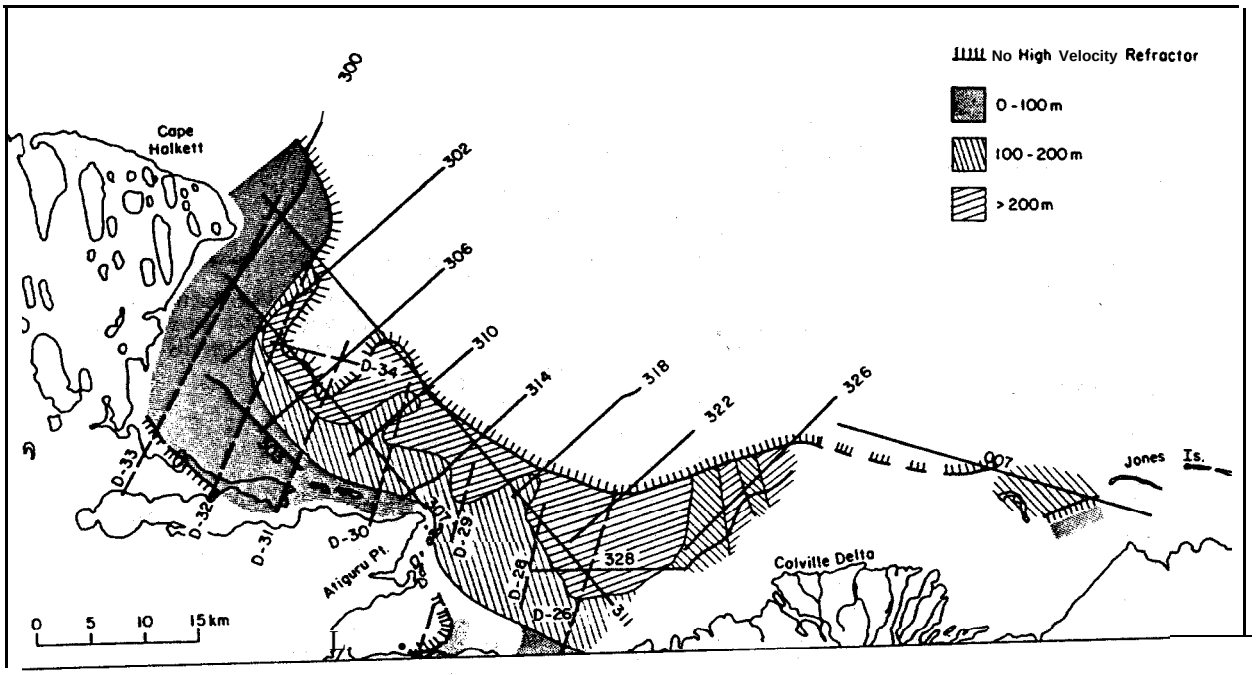

Figure 8. Depth to the top of the high velocity refractor.

layer were ice-bonded coarse-grained material, and the rest of the section were fine-grained with less complete ice-bonding, the usual thick layer of permafrost (300-600 m) could be present.

Velocity profiles and cross sections like those in Figures 5 and 6 were constructed for all the shot lines in Harrison Bay (Appendices B and C). These data suggest the distribution of ice-bonded permafrost when compiled on a set of area maps. The structural zones are shown in Figure 7. A two-layer situation exists in the zone nearest shore, with a high-velocity layer at depth that decreases

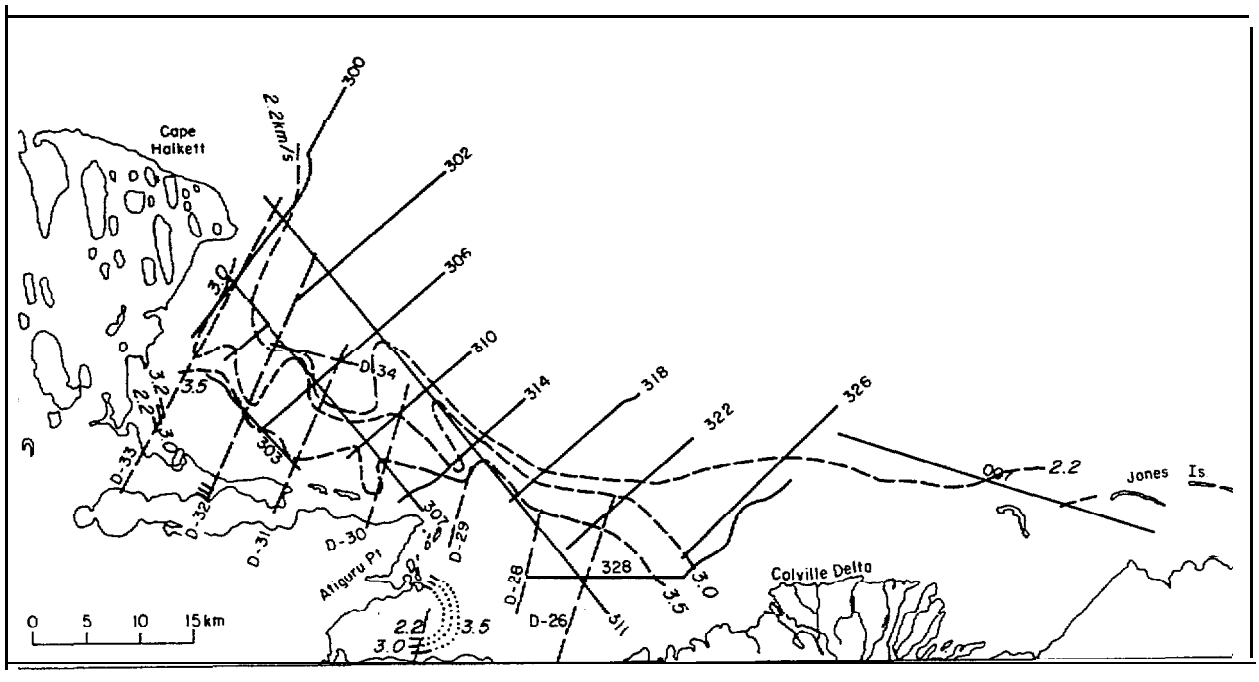

Figure 9. The refraction velocity contours for the high velocity layer.

in velocity and increases in depth with distance from shore. Beyond this zone, the continuation of the high-velocity structure is suggested by a deep reflector. Further offshore, there are no velocities above 2.0 km/s, making it difficult to determine whether the materials are ice-bonded. If they are, the low velocity would indicate that they are warm or have relatively low ice content.

A contour map of the depth to the refractor (Fig. 8) reveals that the high-velocity layer is at or near the surface at the shore and dips to the northeast under the bay. The steepest dips, approximately 3%, are near shore off Atiguru Point and just west of the Colville Delta. Lesser slopes, approximately 1070, are seen further offshore and near the Cape Halkett coastline.

The shallow depth of the refractor observed in the western part of the bay corresponds with observations made to the west near Lonely, which is in the same geological setting. Harrison and Osterkamp (1981) established a probe line offshore from Lonely and observed shallow ice-bonded permafrost 8 to 15 *m* below the seabed out to at least 7.8 km from shore.

A contour map of refractor velocities (Fig. 9) also helps to illustrate the difference between the eastern and western parts of Harrison Bay. Velocities west of Atiguru Point are more variable and decrease more rapidly with distance from shore than velocities east of the point. These differences suggest that a contrast must exist between the material types and also between the geological histories of the two regions. The western part of the bay may have been an extension of the low, lake-covered coastal plain found west of Cape Halkett. The shallow depth of the refractor in this area and the noticeable deerease in velocity with distance from shore would be expected in an area of fine-grained material subject to active coastal retreat.

Attenuation

Figure 10a is a record which illustrates the signature of the air guns and recorder system. It shows an attenuation rate in the sediments which we do not consider anomalous. The dominant frequency of the traces 0.28 km from the source is in the 20- to 40-Hz range. At the far end of the array (2.6 km from the source) the dominant frequency is approximately 20 Hz. In addition, strong high-frequency modes of 80 Hz can be seen as later arrivals on these far traces. Figure 10b shows an anomalous situation where high frequencies are present near the source. Most noticeable is the strong mode at about 80 Hz. The dominant signal at the far end of this array is 10 Hz. A more common type of anomalous record is illustrated in Figure 10c. The entire record, excluding background noise, is composed of frequencies of less than 15 Hz. Similar attenuation is seen on the ice-shooting records (Fig. 10d and 10e). We attribute these anomalies in both the ice and marine records to attenuation in the sediments for a number of reasons. First, the field notes do not indicate any significant air gun malfunctions, and no changes in

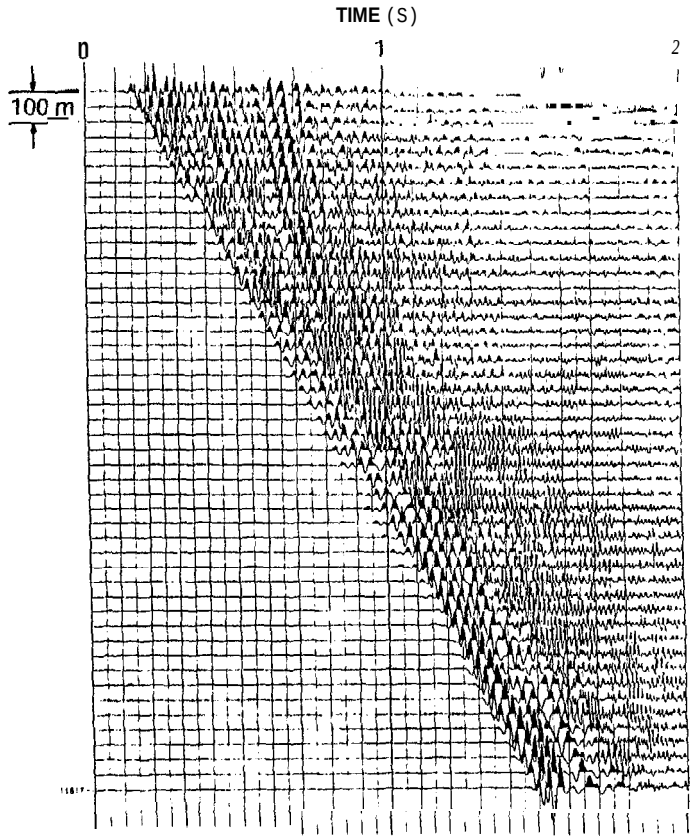

a. A marine record which shows no anomalous attenuation.

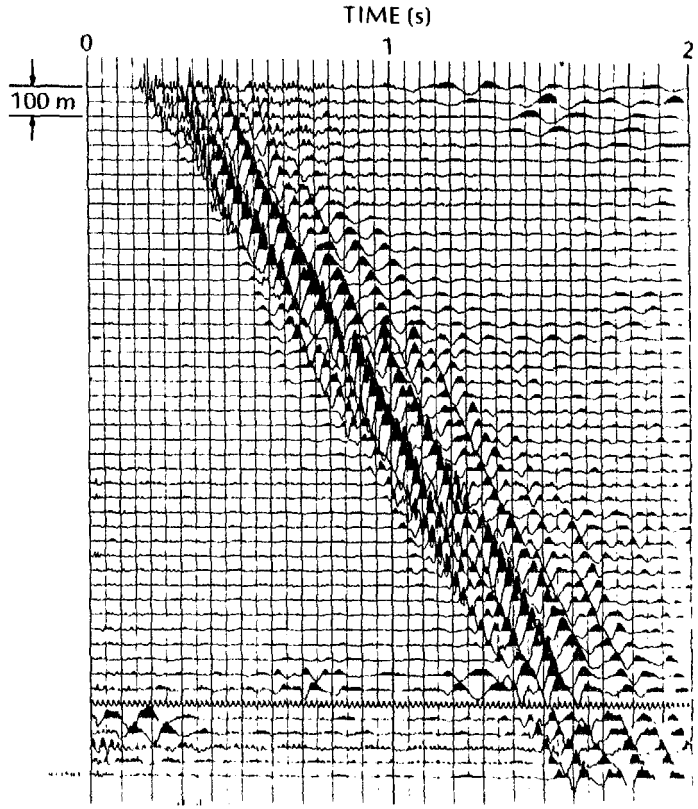

b. A marine record which has high frequencies near the source and a low dominant frequency over the rest of the record.

Figure IO. Sample records for the attenuation study.

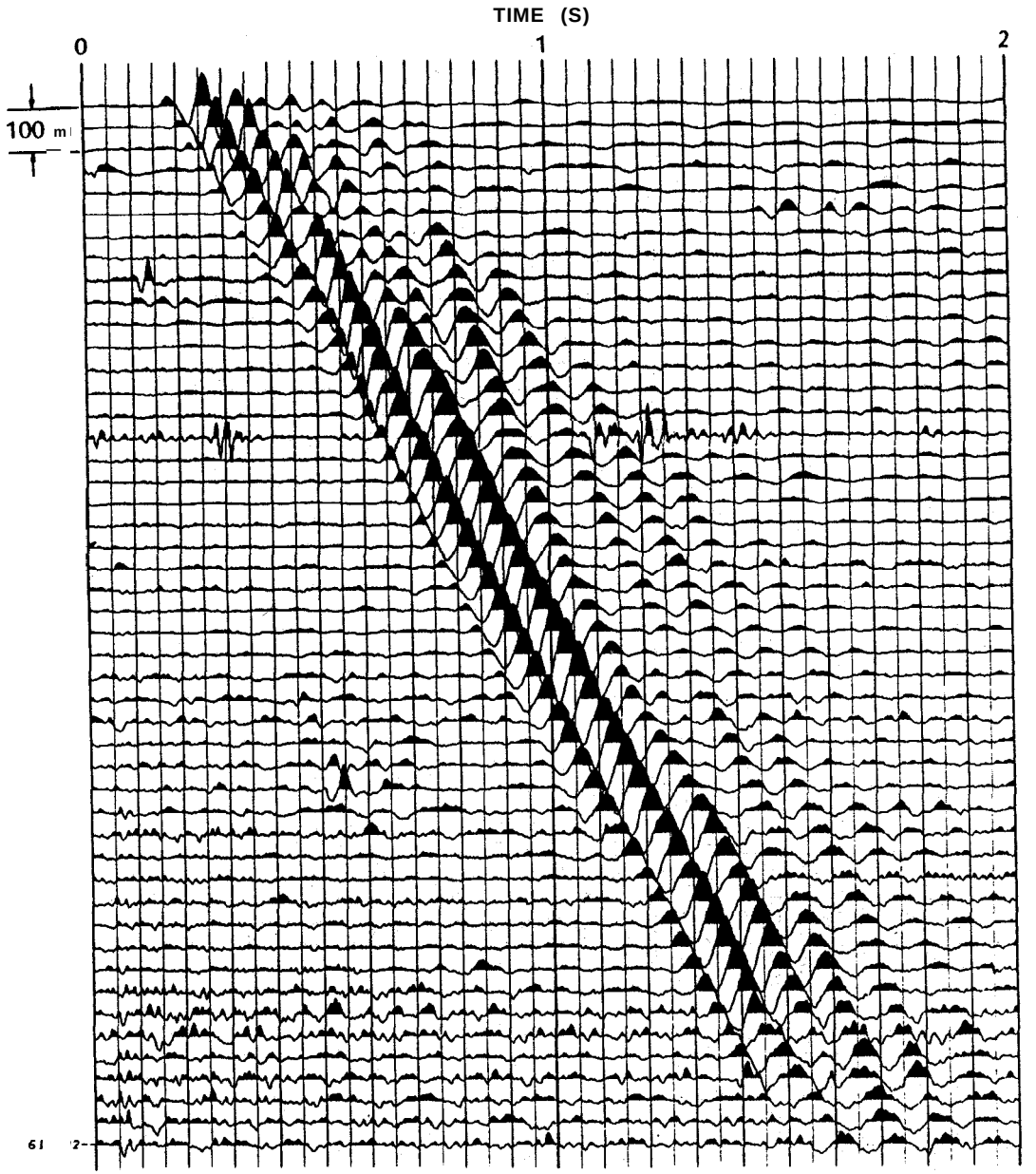

c. A marine record which has a dominant frequency of less than 15 Hz across the whole spread.

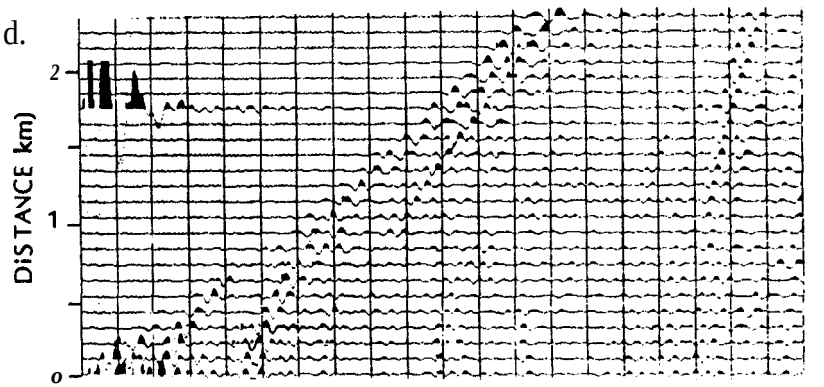

d. An ice-shooting record which shows no anomalous attenuation,

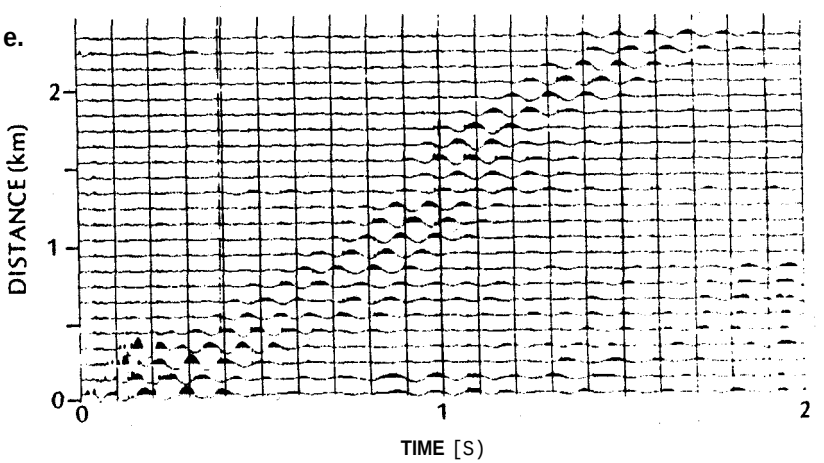

e. An ice-shooting record which has a dominant frequency of less than 15 Hz.

Figure 10 (cent 'd).

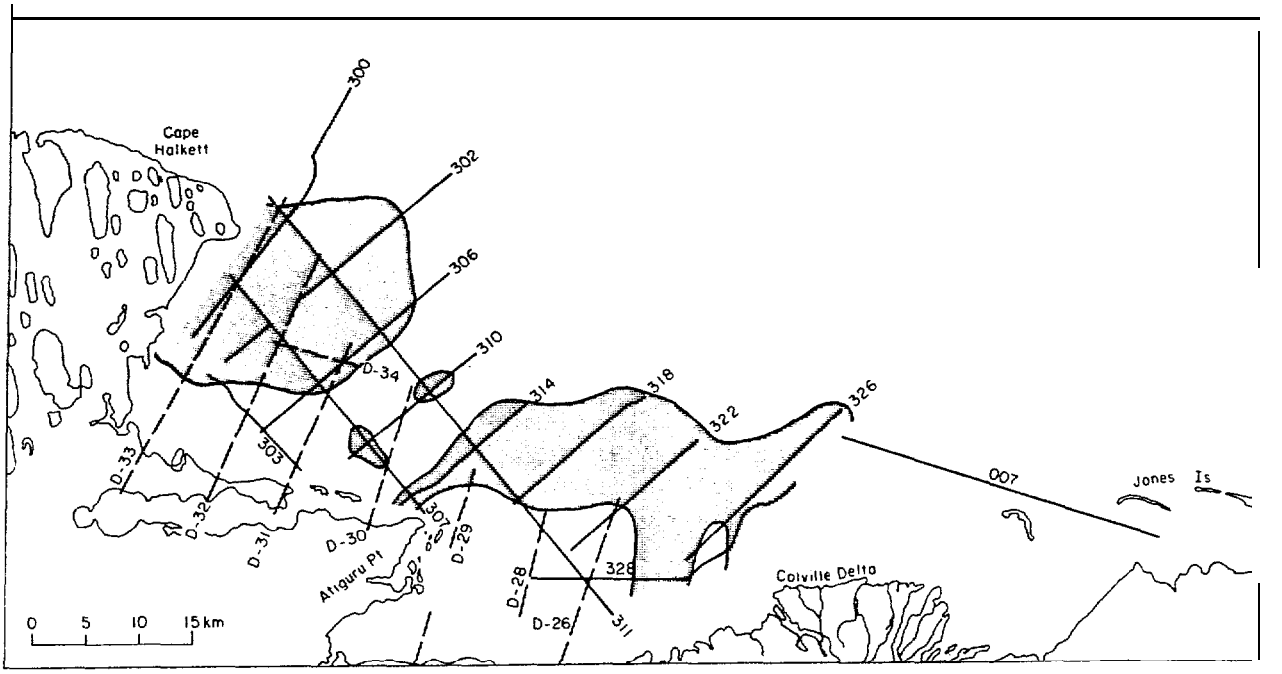

Figure 11. Distribution map of the "shallow gas" anomaly. The high frequency part of the seismic signals has been naturally filtered in the shaded zones.

the recording filters were made. Secondly, these anomalies can be traced from line to line within a survey. Finally, the near-shore extent of the attenuation zones defined by both the marine arid ice shooting surveys are in agreement. This seems to be fairly positive evidence that the anomalies are related to seabed characteristics, since the surveys had different energy sources and were conducted during different times of the year.

The attenuation effect does not appear to diminish the amplitude of the low-frequency end of the spectrum for records such as Figure 10c. This can be explained if these signals constitute the lowest mode in the near-surface waveguide which passes the recorder filter range. There would be no significant energy recorded at any lower frequencies, and these signals would be maintained at nearly constant amplitudes across the record by the automatic gain control of the receiver amplifiers.

Figure 11 outlines the areas where the dominant frequency of the reflected or refracted signals was reduced from approximately 30 Hz to less than 15 Hz. These areas are of considerable interest because strong attenuation has been associated with the presence of gas in the pores of sediments. Laboratory studies by W inkier and Nur (1979) have shown that pore gas concentrations as low as a few percent by volume can cause attenuation to increase by a factor of 5 over water-saturated values. Therefore, the high attenuation observed on Harrison Bay records could be explained by the presence of natural gas in the sediments. Shallow gas has been reported near Prudhoe Bay by Boucher et al. (1981), based on the results of high resolution seismic studies. It has also been observed in the Canadian Beaufort Sea off the Mackenzie Delta by Neave et al. (1978), based on evidence from drilling and seismic studies. As a result, we feel that there is considerable evidence that the attenuation zones in Figure 11 can be viewed as the shallow gas distribution for Harrison Bay.

The depth of the gas deposits has not been determined. However, the attenuated signals from both refraction and reflection analysis penetrate to depths in the range 20 to 400 m. Consequently, the gas deposits must lie in this range.

According to the stability conditions for gas hydrates, a solid form of natural gas and water can be found in permafrost at a depth of 100 m or greater, depending on the composition of the gas (Davidson et al. 1978, APOA 1978). Therefore, there could be some gas in hydrate form within and below the ice-bonded layer in these areas of shallow gas.

The proposed gassy zone in Figure 11 covers a large portion of the area in Figure 9, where apparently active degradation of ice-bonded permafrost is taking place, suggesting a direct relationship between the two zones. The source of the gas

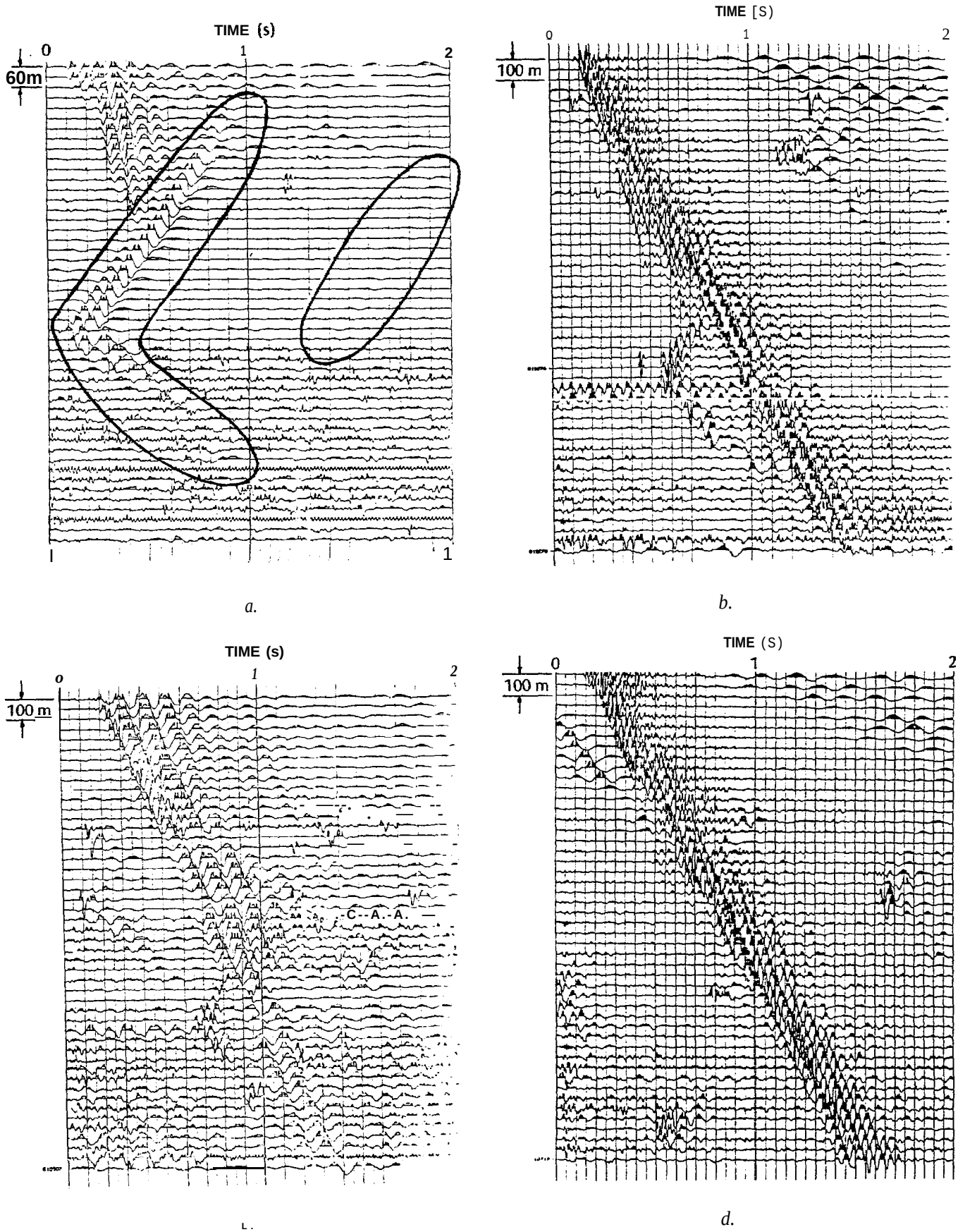

Figure 12. Examples of seismic noise on marine records. a-d} Records from north of Sagavanirktok River and Tigvariak Island.

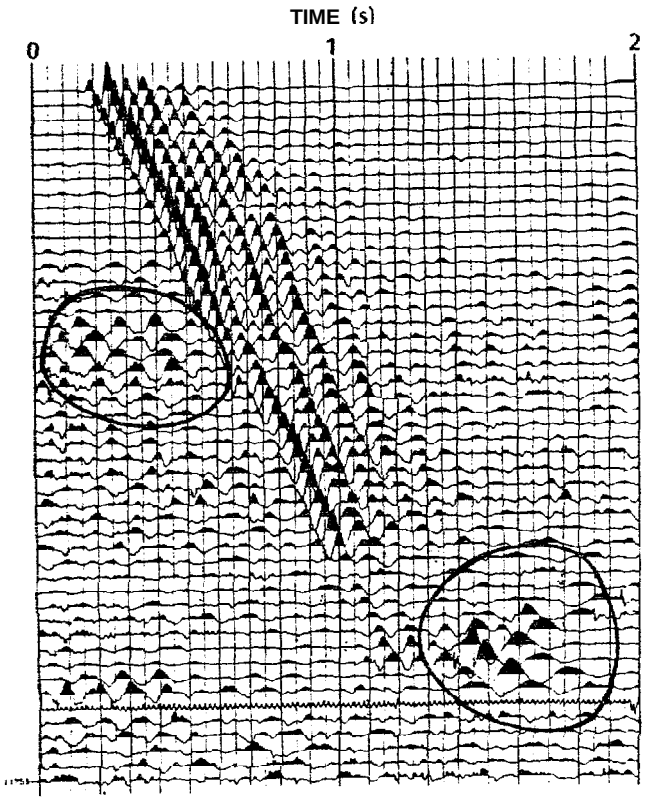

e.

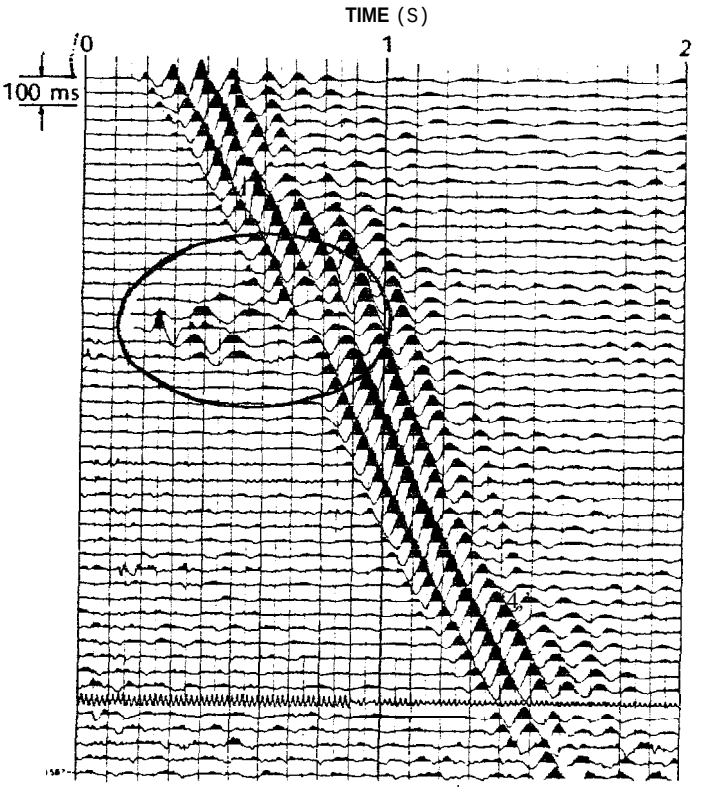

f.

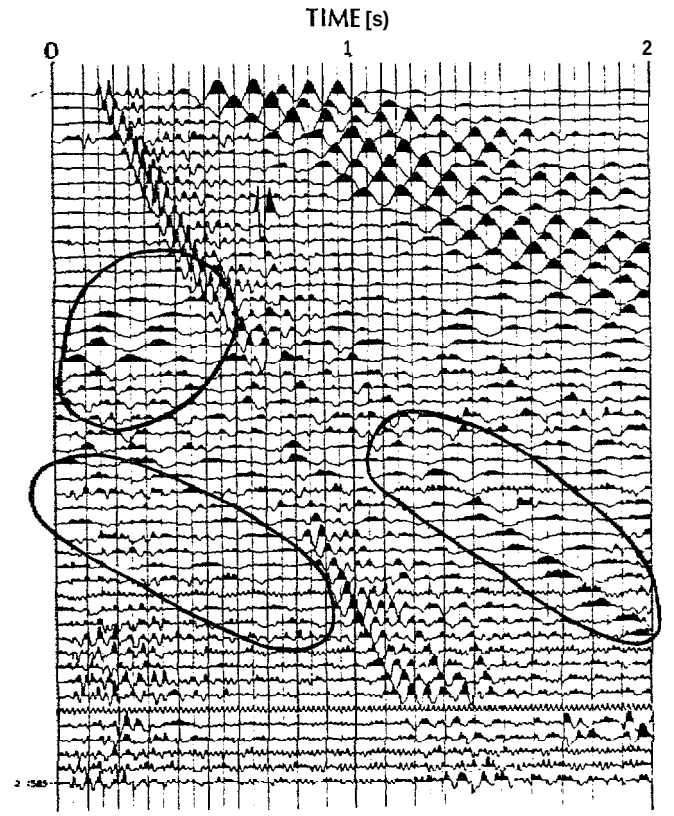

g.

Figure 12 (cent'd) Examples of seismic noise on marine records. e-g) Records from Harrison Bay. These events are not as strong and show more dispersion than the ones from the eastern areas (a-d).

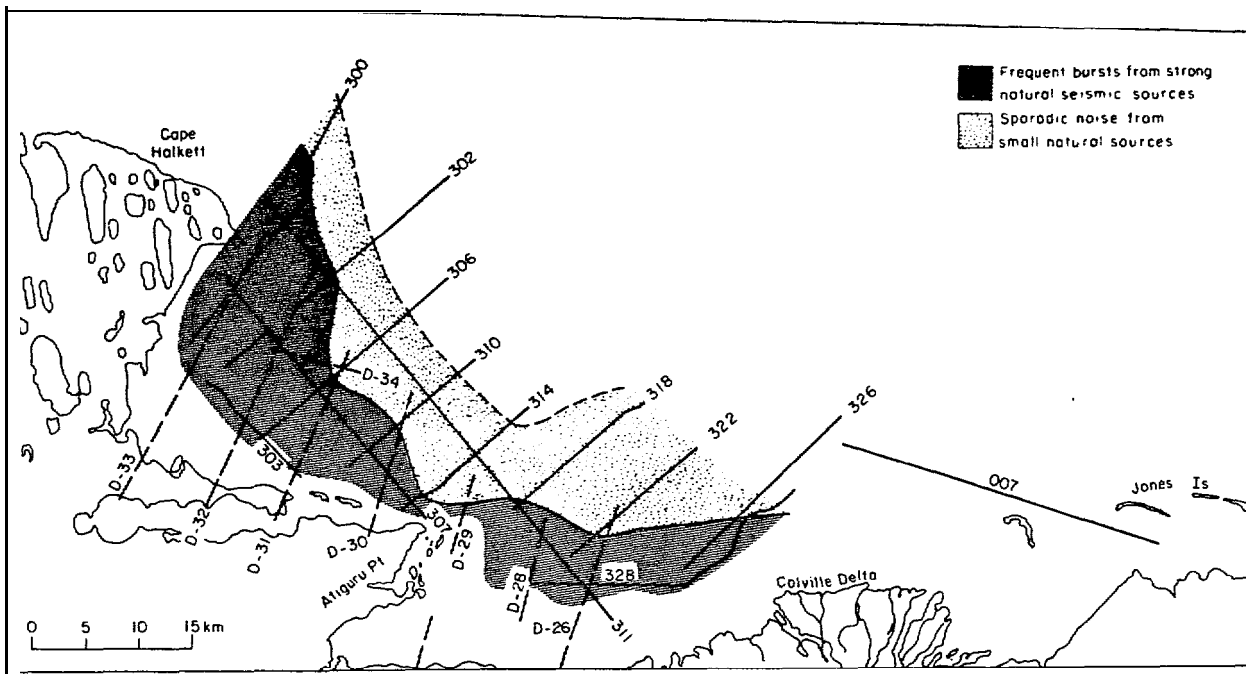

Figure 13. *The distribution of natural seismic activity in Harrison Bay. The strongest events and highest activity are in a band close m shore.*

is unknown. It may be biogenic gas formed in place or it may be from depth, freed by thawing of impermeable zones, or from decomposition of hydrates.

Low-level natural seismicity

Most of the noise on the records examined as part of this study seems to be a form of natural seismicity associated with areas of shallow subsea permafrost. The best examples were observed in the Sagavanirktok Delta and Tigvariak Island area just east of Prudhoe Bay. Similar events were found in Harrison Bay. Figures 12a-d reproduce four of the clearest events from the records east of Prudhoe. They are not found at any particular place or time on the records. The Harrison Bay events (Fig. 12e-g) are similar, aside from the fact that they have more dispersion and low amplitudes. A good correlation of the activity turns out to be with the distribution of ice-bonded permafrost. However, the prospect that this noise may be generated by some other feature, such as ice movement, cannot be discounted.

Regions in which seismic events were observed are shown in Figure 13. These regions correspond with both the location of the high-velocity materials and the regions of shallow gas. The noise could be related to energy released during permafrost degradation. In such a process, the energy could originate from expanding gas or adjustment of seabed material to differential settlement caused by permafrost thaw.

Figure 14 compares the phase velocity of Rayleigh waves from the air guns with the phase velocities of the induced seismicity for Line 311. They both lie in the same velocity range (0.3 to 1.1 km/s), which is below the compressional wave velocity in water (1.4 km/s) and also much less than the plate wave velocity in sea ice (2.5-3.0 km/s). This observation helps to confirm that the noise is associated with the sediments and not with waves or ice. The group velocities (not shown) are less than the phase velocities, so their dispersion is like Rayleigh wave normal modes. Therefore, the measured phase velocities lie between the Rayleigh wave velocities of the thawed layer and the frozen layer. See Ewing et al. (1957), for a discussion of these velocities.

The amplitudes of these signals cannot be determined due to automatic gain control on the recording equipment. However, they appear to have an energy output similar to that of the air guns. Because there are no recordings without air-gun shots, it is not clear whether or not the noise was triggered by the shots, like the aftershocks that occur in land seismic data in permafrost. In any case, the noise suggests that unstable conditions are present in areas of actively degrading permafrost.

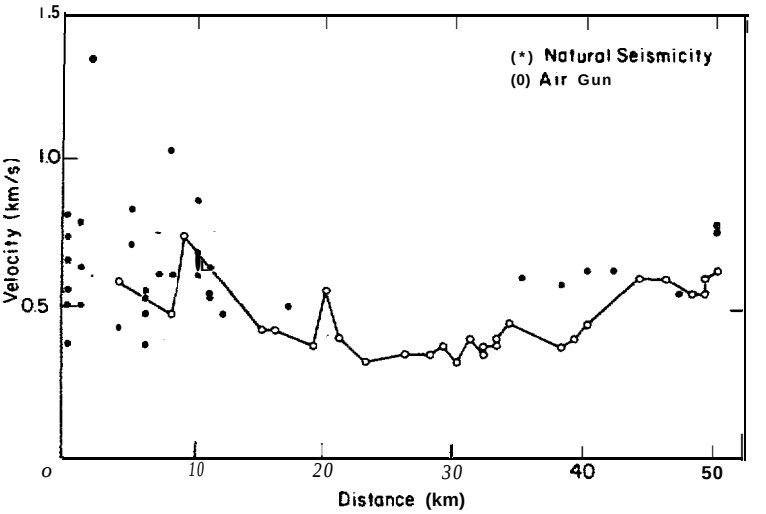

Figure 14. Phase velocities from natural signals compared to the phase velocity of surface waves from the air guns for Line 311.

SUMMARY

Velocity profiles for Harrison Bay show that high-velocity material interpreted as ice-bonded permafrost is common in this region. The high-velocity ice-bonded sediments extend at least 25 km from shore. There is a considerable variation in the apparent permafrost distribution, which indicates the significant effect of material types, past inundation and geological history on the rate of subsea permafrost degradation. In particular, the part of the bay west of Atiguru Point is more chaotic in terms of velocity and depth variations. The eastern half of the bay has far more regular permafrost profiles. Across the whole northern edge of the study area, it appears that thermal degradation has modified the bonded permafrost to depths as great as 300 m.

The anomalous attenuation on the seismic records observed in Harrison Bay was interpreted as an indicator of free gas in the section above the frozen sediments. This means that gas hydrates can occur at greater depths and may be the source of the free gas liberated as permafrost thawed.

The swarms of small quakes or seismic noise observed in the nearshore areas were interpreted as energy released due to thermal modification of this recently inundated permafrost.

LITERATURE CITED

APOA (1978) A review of oil industry experience with gas hydrates in exploratory drilling in the Canadian Arctic. Prepared by APOA Drilling Subcommittee for the Symposium on Permafrost Geophysics, National Research Council of Canada.

Aptikaev, F.F. (1964) Temperature field effect on the distribution of seismic velocities in the permafrost zone. In: Akademiia Nauk SSSR, Sibirskoe Otdelenie, Inst. Merzlotovedenii, Teplovye Protsessy v Merzlykh Gruntakh.

Barnes, P.W. and D.M. Hopkins (1978) Geological sciences. In: *Interim Synthesis: Beaufort/Chukchi Sea, Environmental Assessment of the Alaskan Continental Shelf,* p. 101-133.

Boucher, G., E. Reimnitz and E. Kempema (1981) Seismic evidence for an extensive gas-bearing layer at shallow depth, offshore from Prudhoe Bay, Alaska. *Cold Regions Science and Technology, vol. 4,* no. 1, p. 63-71.

Davidson, D. W., M.K. El-Defrawy and M.O. Fuglem (1978) Natural gas hydrates in nort hem Canada. In *Proceedings III International Conference on Permafrost.* National Research Council of Canada, Ottawa, p. 938-943.

Ewing, W. M., W.S. Jardetzky and F. Press (1957) *Elastic Waves in Layered Media.* New York: McGraw-Hill, 380 p.

Grant, F.S. and G.F. West *(1965) Interpretation Theory in Applied Geophysics. New* York: McGraw-Hill.

Harrison, W .D. and T.E. Osterkamp (1981) Subsea permafrost: Probing, thermal regime and data analysis. Environmental Assessment of the Alaskan Continental Shelf, Annual Reports of Principal Investigators (NOAA-BLM).

Hunter, J. A., **A.S. Judge, H.A. MacAulay, R.L. Good, R.M. Gagne and R.A. Burns (1976'**

Permafrost and frozen sub-seabottom materials in the southern Beaufort Sea. Geological Survey of Canada, Ottawa, Beaufort Sea Project Technical Report 22.

Jakosky, J .J. (1940) *Exploration Geophysics.* Newport Beach, California; Trija, 1195 p.

Neave, K. G., A.S. Judge, J.A. Hunter and H.A. MacAulay (1978) Offshore permafrost distribution in the Beaufort Sea as determined from temperature and seismic observation. In Current Research, Part C, Geological Survey of Canada, Paper 78-1C, p. 13-18.

Rogers, **J.C.** and **J.L. Morack** (1981) Beau fort and Chukchi seacoast permafrost studies. Environmental Assessment of the Alaskan Continental SheIf, Annual Report.

Sellmann, P. V., **E.J. Chamberlain, K.G. Neave and A. Delaney (1980)** Delineat ion and engineering characteristics of permafrost beneath the Beaufort Sea. Environmental Assessment of the Alaskan Continental Shelf, Annual Report, vol. IV, p. 125-157.

Sherwood, J.W.C. (1967) Refraction along an embedded high-speed layer. In: *Seismic Refraction Prospecting* (A. W. Musgrove, Ed.). Society of Exploration Geophysicists, Washington, **p.** 138-151.

Winkler, K, and **A. Nur (1979)** Pore fluids and seismic attenuation in rocks. *Geophysical Research Letters, vol.* **6,** no. 1, p. **1-4.**

Yerkes, R.F. and **R.O. Castle** (1976) Seismicity and faulting attributable to fluid extraction, *Engineering Geology,* vol. 10, no. **2-4,** p. **151-168.**

APPENDIX A: ERROR ESTIMATES

The first error estimate arises from using an average upper layer velocity of 1.8 km/s for refraction calculations instead of the local value. A worst case situation is examined to illustrate how much error is introduced. The remaining error problems involve dipping layers when the interpretation assumes horizontal layers. For these cases, we used typical readings and calculated the difference between the velocity and depth estimates for horizontal layers and layers with a 3% dip.

When the correct local velocity V_1 is used in eq 8 of the *Methods* section, the depth is:

$$h_L = (t - x/c)\,(V_L/2)\,[1 - (V_L/V_1)^2]^{-1/2}. \quad (13)$$

When the average velocity V_A = 1.8 km/s is used instead, the erroneous depth estimate is

$$h_A = (t - x/c)\,(V_A/2)\,[1 - (V_A/V_1)^2]^{-1/2}. \quad (14)$$

The proportional error in the depth estimate is

$$(h_L - h_A)/h_L = 1 - h_A/h_L$$

$$= 1 - \frac{V_A}{V_L}\left[\frac{1 - (V_L/V_1)^2}{1 - (V_A/V_1)^2}\right]^{1/2}. \quad (15)$$

This expression gives the largest error when the local velocity is large and the lower layer velocity V_1 is small. From the velocity histogram in Figure 4, we can choose V_L = 2.0 km/s and V_1 = 3 km/s. This highly unlikely combination of velocities results in an error of 30%.

The effects of dip on the interpretation of apparent lower layer velocity from single-ended refraction data can be found from eq 1:

$$c = V_0/\sin[\sin^{-1} \text{WOW,}) + \psi]. \quad (16)$$

The real veloicty in the lower layer can be found by solving this equation for VI:

$$V_1 = V_0/\sin[\sin^{-1}(V_0/c) - \#]. \quad (17)$$

The proportional error in the lower velocity from using a horizontal layer model is

$$(V_1 - c)/V_1 = 1 - c/V_1$$

$$= 1 - (c/V_0)\,\sin[\sin^{-1}(V_0/c) - 0]. \quad (18)$$

The estimated depth for the horizontal layer model is given by eq 8:

$$h_H = (V_0/2)\,(t - x/c)\left[1 - (V_0/c)^2\right]^{-1/2}. \quad (19)$$

'Ibis equation can have V_1 replaced by a substitution from eq 17.. Then eq 19 and 20 can be used to find the proportional error in the depth:

$$(h_D - h_H)/h_D = 1 - \cos[\sin^{-1}(V_0/c) - \phi]\left[1 - (V_0/c)^2\right]^{-1/2}. \quad (20)$$

Using a typical set of velocities, V_0 = 1.8 km/s and c = 3.66 km/s. A dope of 3% results in a 2% error in depth according to eq 21, and the corresponding error in the velocity is 5% from eq 18.

For the reflections from a plane boundary which dips at an angle #J, the arrivals on the record still form a hyperbolic curve; however, the hyperbola is not centered with respect to the shot point. The arrival times can be calculated from an image source R (Fig. Al) which is at a depth $\zeta = 2h \cos\phi$ and displaced by a horizontal distance $\xi = 2h \sin\phi$ from the true source P.

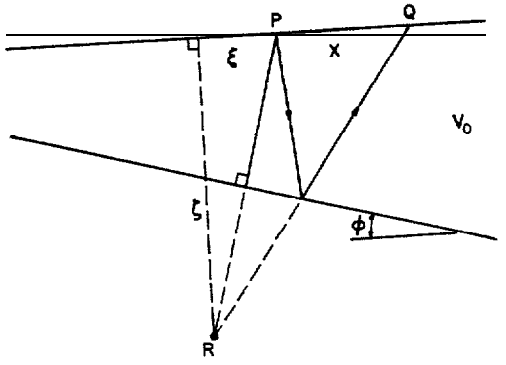

Figure A1. Ray path geometry for a reflector dipping at an angle ϕ.

The travel time equation is

$$t^2 = \frac{(x + \xi)^2 + (2h\cos\phi)^2}{V_0^2}$$

$$t^2 = (1/V_0^2)\,(4h^2\cos^2 \# + 4h^2\sin^2\phi + 4hx\sin\phi)$$

$$t^2\,V_0^2 = 4h^2 + x^2 + 4hx\sin\phi\,. \qquad (21)$$

Taking differentials on both sides of the equation gives

$$2t\,V_0^2\,dt = 2x\,dx + 4h\sin\phi\,dx$$

$$V_0^2 = (x/t)\,(dx/dt) + (2h\sin\phi/t)\,(dx/dt)\,. \qquad \mathbf{(22)}$$

The estimated velocity for the horizontal layer interpretation was

$$V_H = \left(\frac{x\,dx}{t\,dt}\right)^{1/2} = \left(\frac{cx}{t}\right)^{1/2}\,. \qquad \mathbf{(23)}$$

This can be substituted into eq 23:

$$V_0^2 = V_H^2 + 2h\sin\phi\,V_H^2/x$$

$$V_0 = V_H\,[1 + 2h\sin\phi/x]^{1/2}\,. \qquad (24)$$

The proportional error in velocity is

$$(V_0 - V_H)/V_0 = 1 - [1 + 2h\sin\phi/x]^{-1/2}\,. \qquad (25)$$

Now compare the horizontal layer depth estimate in eq 12

$$h_H = (x/2)\ [(et/x) - 1]^{1/2}$$

to the distance to reflector in eq 22

$$t^2 V^2 = 4h^2 + x^2 + 4h \times \sin\phi .$$

To eliminate V_0, we use eq *24* and 25:

$$ctx\,[1 + (2h \sin\phi/x)] = 4h^2 + X2 + 4hx \sin\phi .$$

This is rearranged as a quadratic equation with h as the unknown:

$$4h^2 + (4x \sin\phi - 2ct \sin\phi)\, h + x^2 - ctx = 0 . \qquad (26)$$

Solving for h gives

$$h_d = (1/8)\ (2ct - 4x)\ \sin\phi \pm (1/8)\ \left[(2ct - 4x)^2 \sin^2\phi - 16\ (X^2 - ctx)\right]^{1/2}$$
$$= [(ct/4) - (x/2)] \sin\phi \pm (1/4)\ [(et - 2x)^2 \sin^2\phi - 4(x^2 - ctx)]^{1/2}. \qquad (27)$$

The relative error in depth is

$$\frac{h_d - h_H}{h_d} = 1 - \frac{(x/2)\ [(et/x) - 1]^{1/2}}{1/4\ (et - 2x) \sin\phi \pm 1/4\left[(et - 2X)^2 \sin^2\phi - 4x(x - et)\right]^{1/2}} \qquad (28)$$

For a typical reflection reading, c = 2.0 Ian/s, x = 1.0 km and t = 0.63s. With a dip of 3% on the reflector, we find a 1% error in the velocity determination and a 2% error in the depth.

APPENDIX B: VELOCITY PROFILES

The following profiles are plotted with south on the left. The velocity decreases consistently from left to right except on Line 303, which is parallel to the strike of the structure. Where there are two profiles the low-velocity profile is the near-surface velocity. h two cases, Lines 307 and 311, the velocity rises at the right end of the line. The right ends of these lines approach the coast near Cape Halkett.

Both refraction and reflection velocities are plotted on most of the following lines. Refraction data are indicated by (+) and reflection data by (0).

The profiles are identified by a line number. The location of these lines in Harrison Bay can be found in Figure 1.

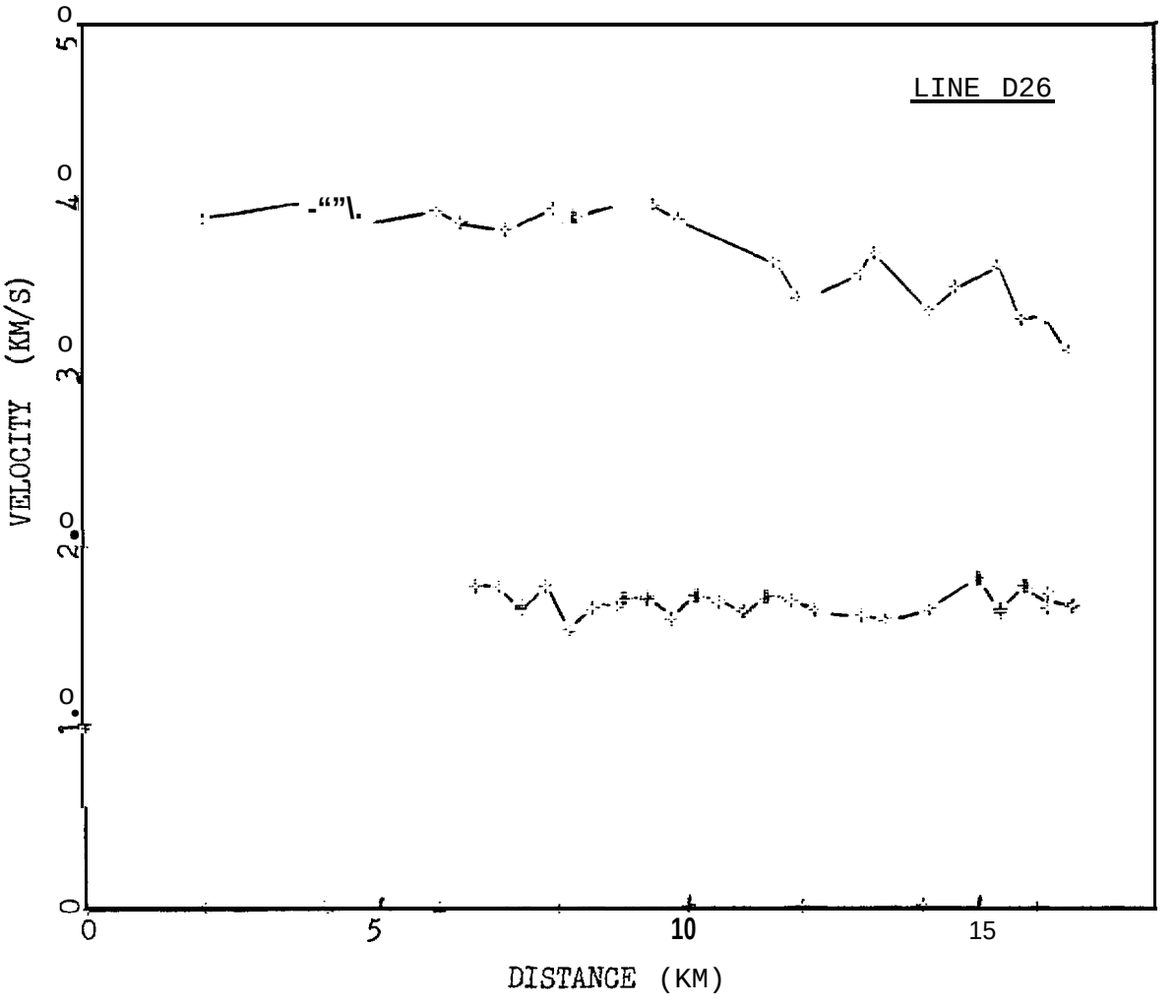
LINE D26
VELOCITY (KM/S)
5.0
4.0
3.0
2.0
1.0
0
0
5
10
15
DISTANCE (KM)

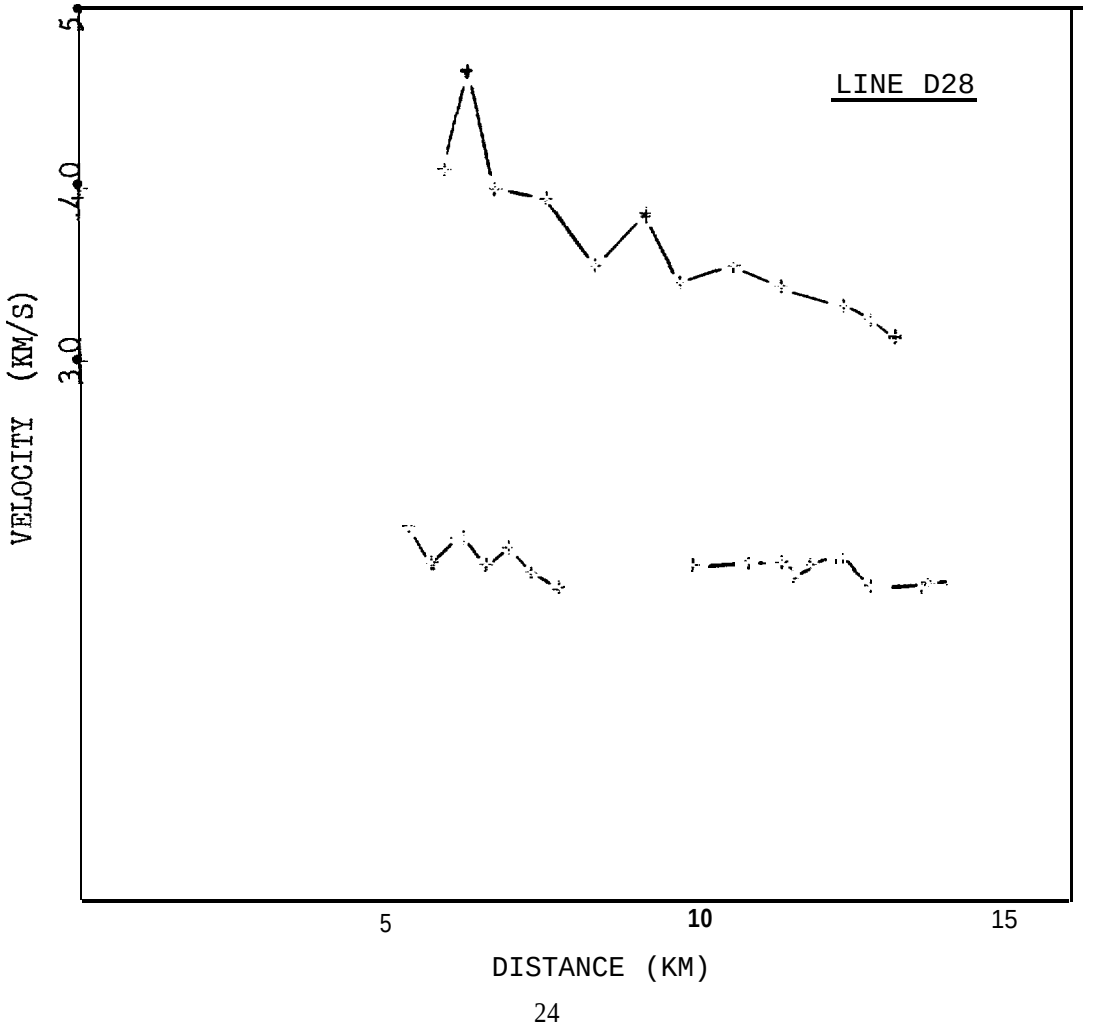
LINE D28
VELOCITY (KM/S)
5.0
4.0
3.0
5
10
15
DISTANCE (KM)

LINE D29
VELOCITY (KM/S)
1.0
2.0
3.0
4.0
5.0
DISTANCE (KM)
20

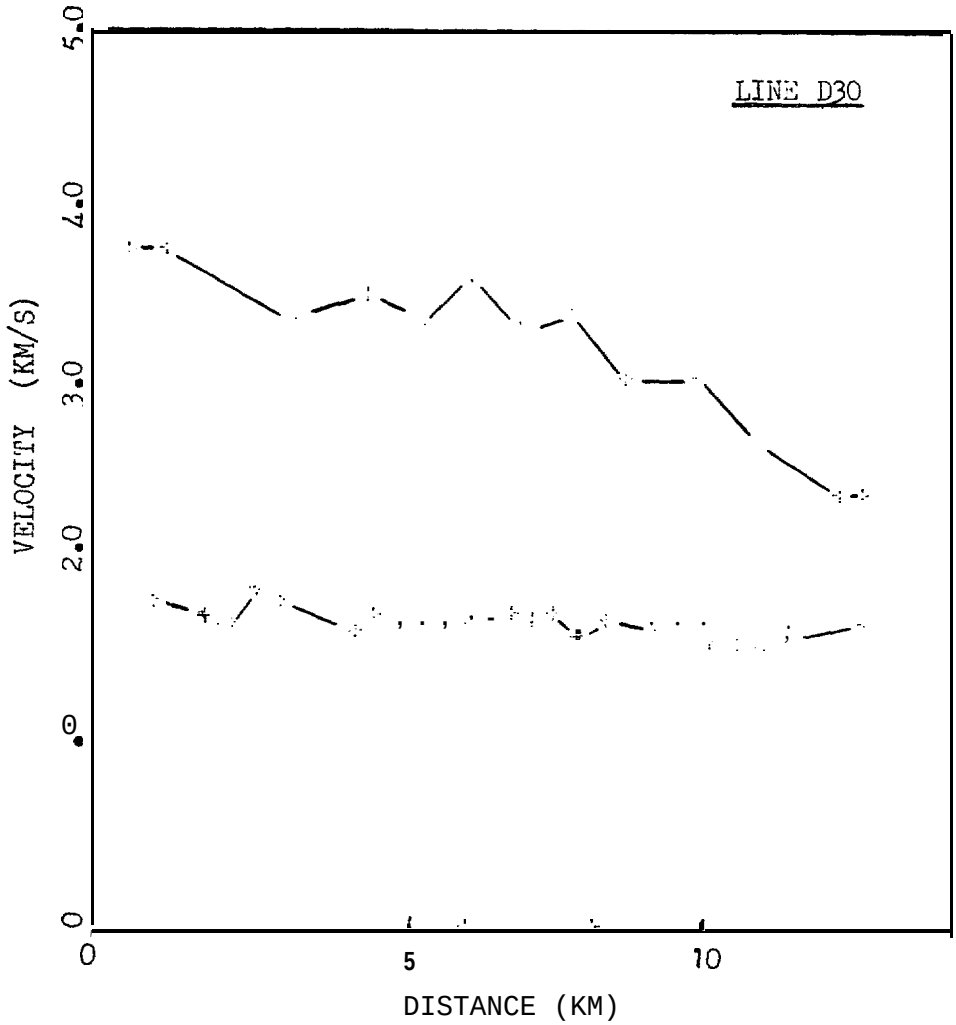
LINE D30
VELOCITY (KM/S)
5.0
4.0
3.0
2.0
0
0
5
10
DISTANCE (KM)

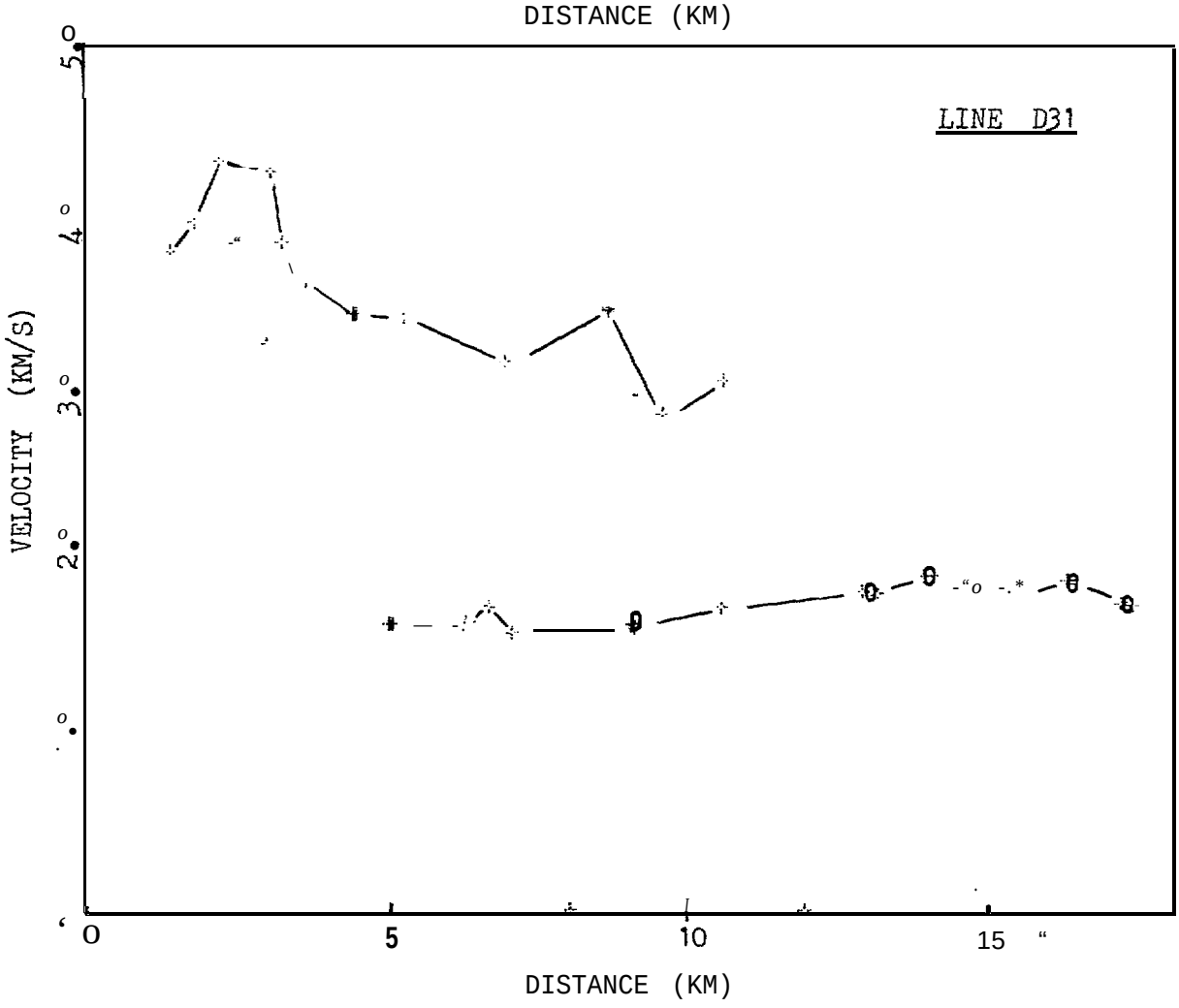
LINE D31
VELOCITY (KM/S)
5
4
3
2
0
0
5
10
15
DISTANCE (KM)

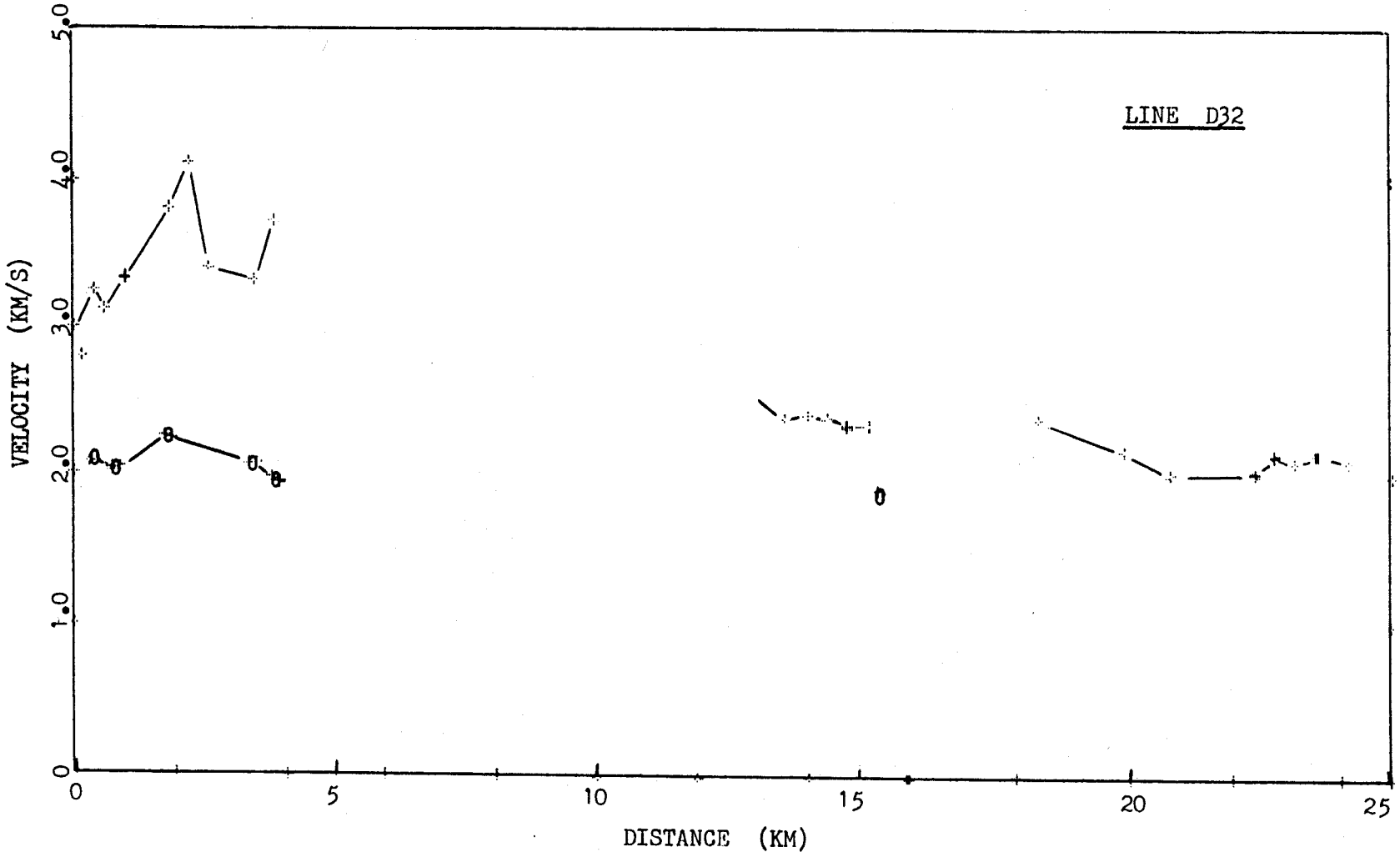
LINE D32
VELOCITY (KM/S)
0
1.0
2.0
3.0
4.0
5.0
0
5
10
15
20
25
DISTANCE (KM)

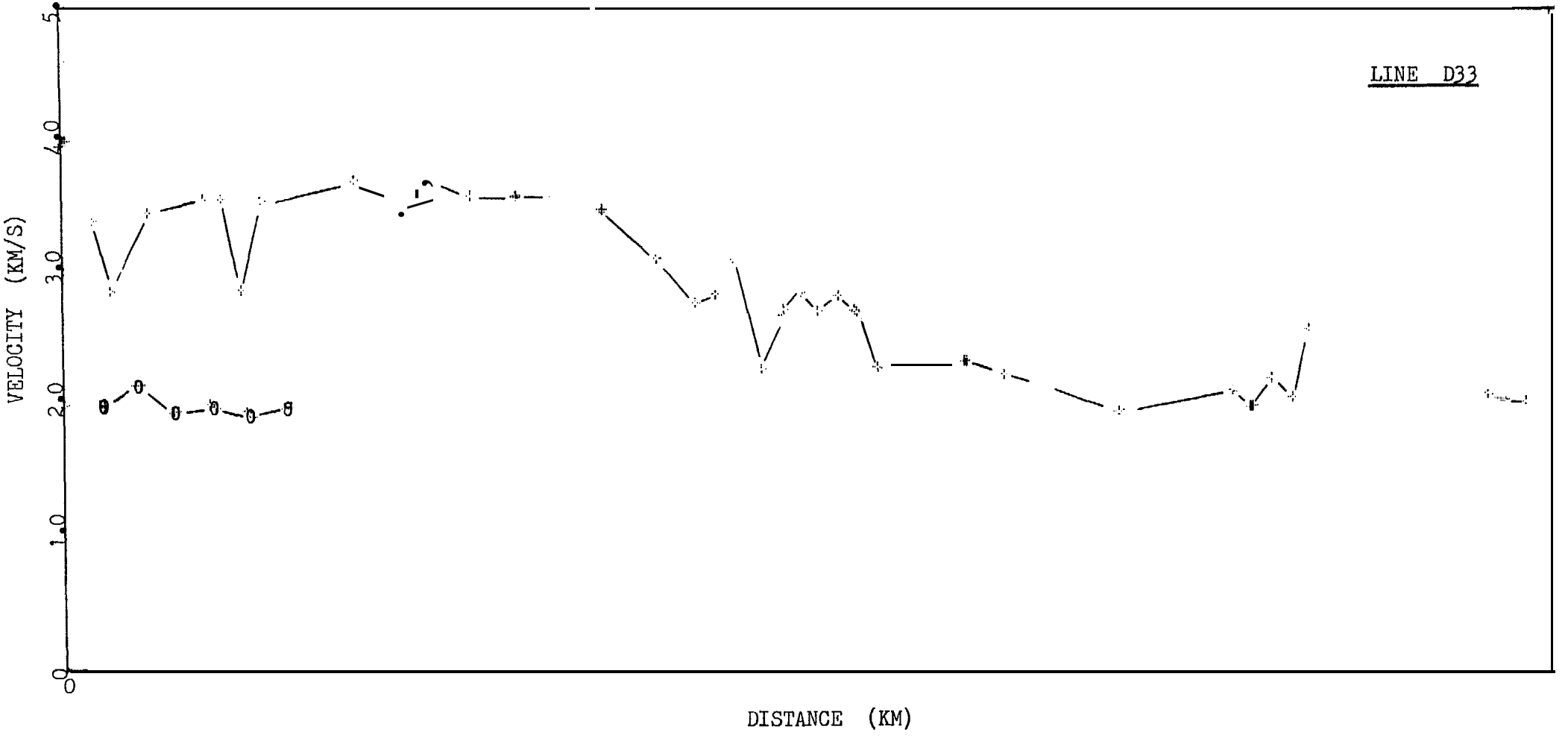
LINE D33
VELOCITY (KM/S)
0
1.0
2.0
3.0
4.0
5.0
0
DISTANCE (KM)

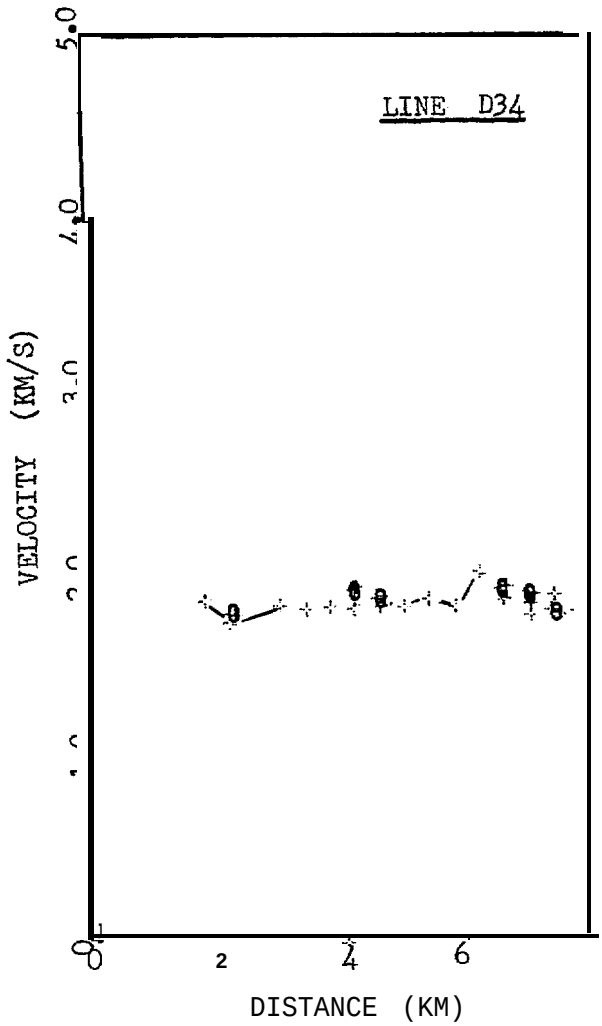
LINE D34
VELOCITY (KM/S)
5.0
4.0
3.0
2.0
1.0
0.0
0
2
4
6
DISTANCE (KM)

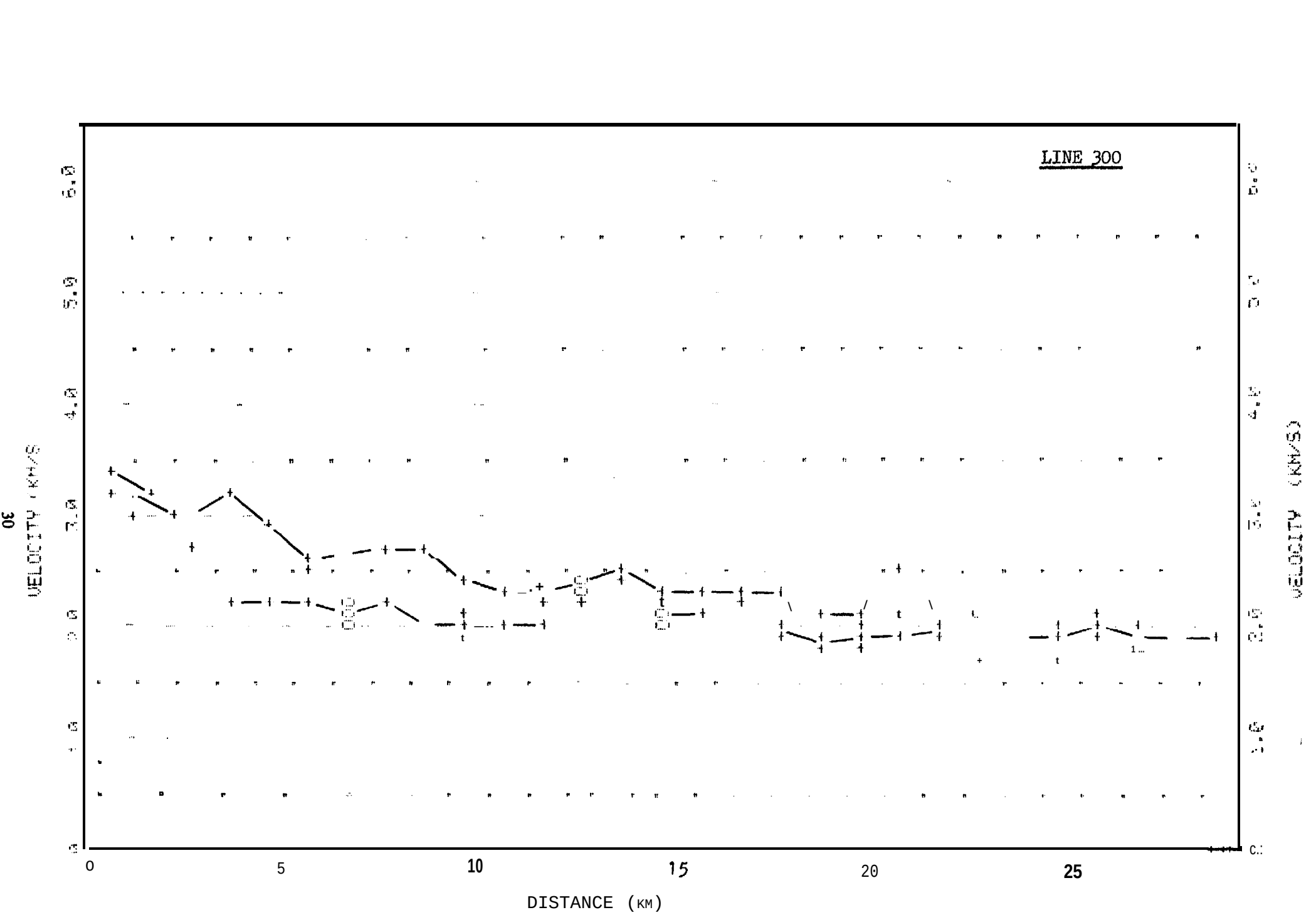
LINE 300
VELOCITY (KM/S)
DISTANCE (KM)
0
5
10
15
20
25

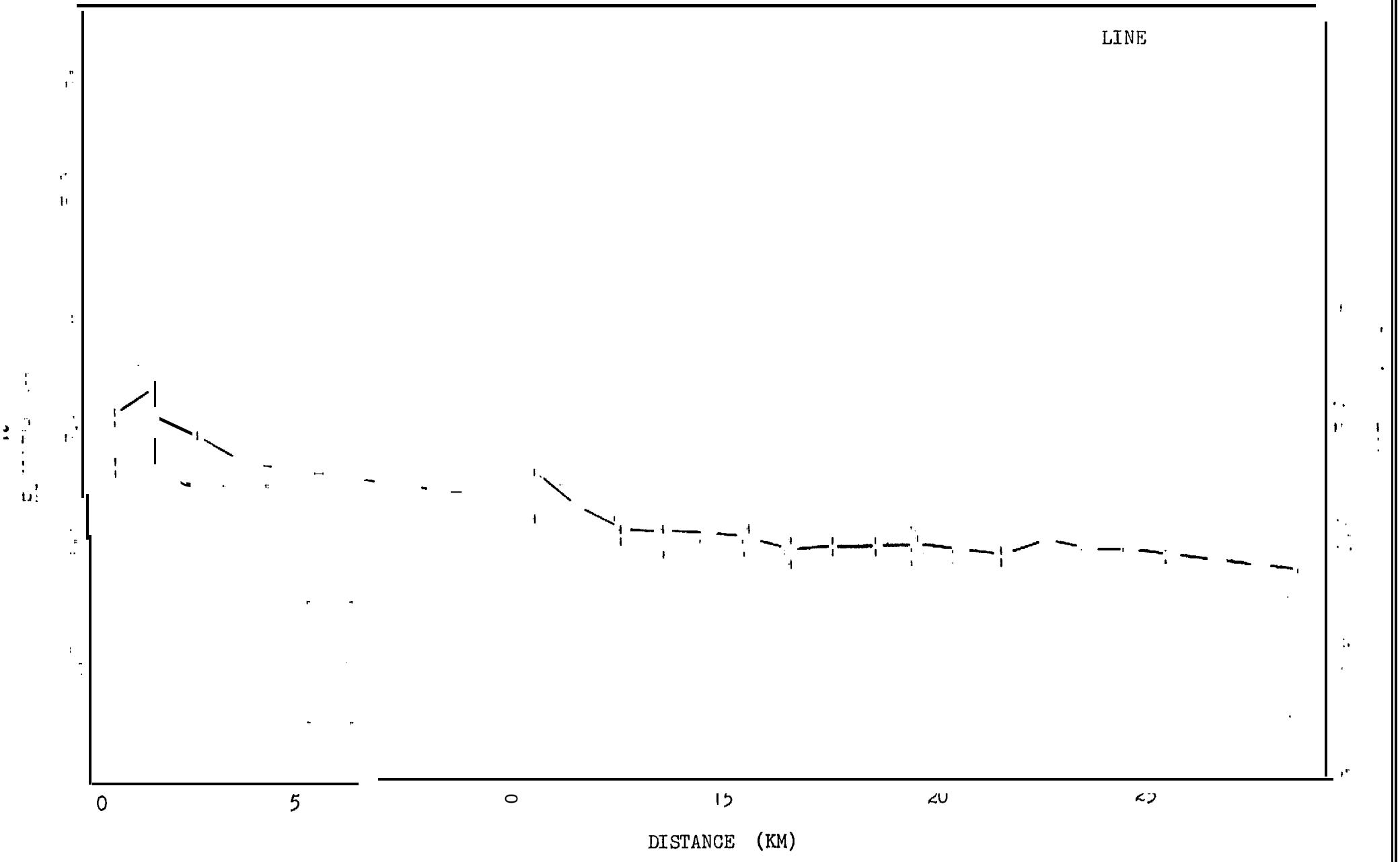
LINE
0
5
0
15
20
DISTANCE (KM)

LINE 306
VELOCITY (KM/S)
0
1.0
2.0
3.0
4.0
5.0
6.0
DISTANCE (KM)
0
1
2

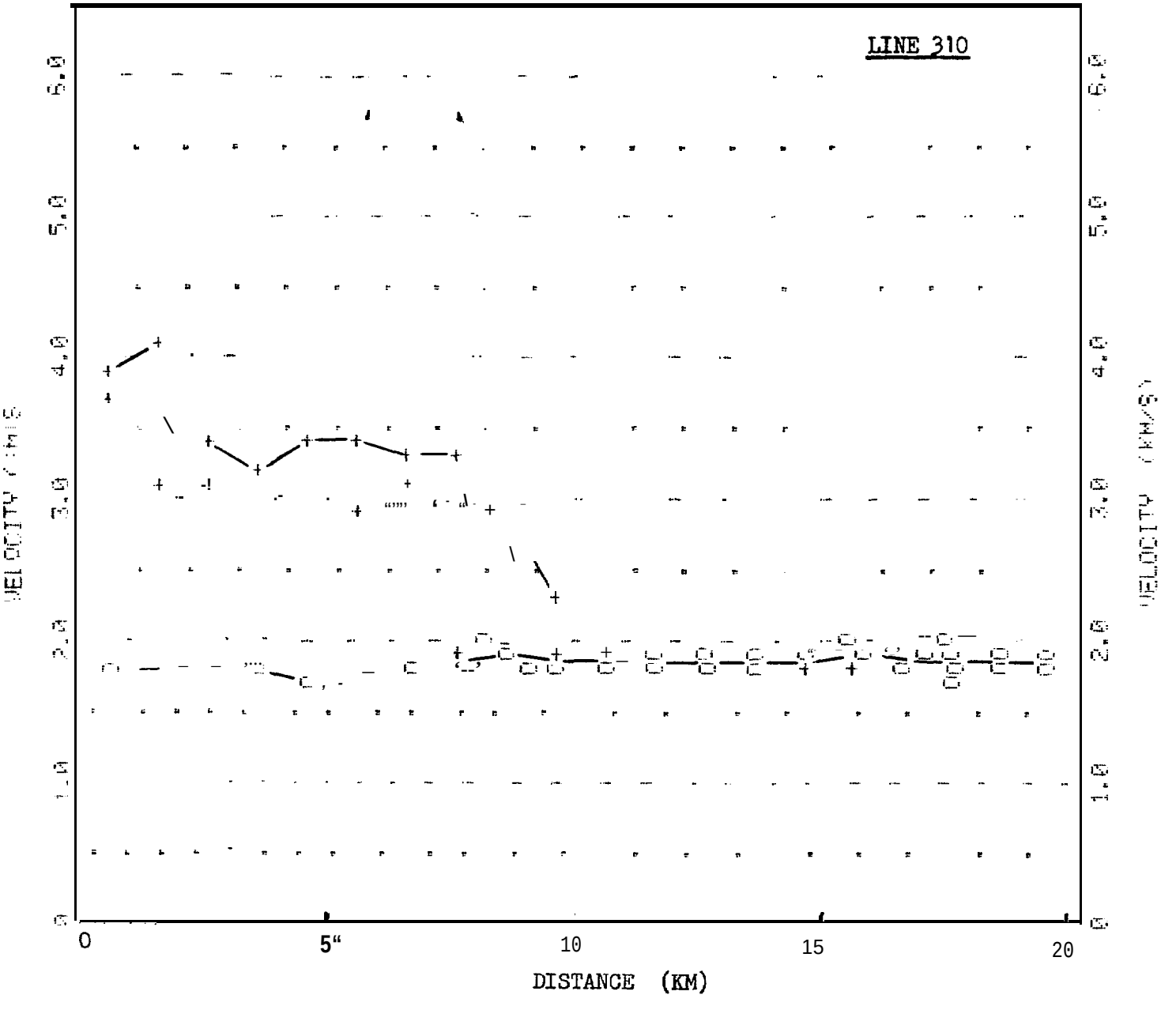
LINE 310
VELOCITY (KM/S)
6.0
5.0
4.0
3.0
2.0
1.0
0
0
5
10
15
20
DISTANCE (KM)

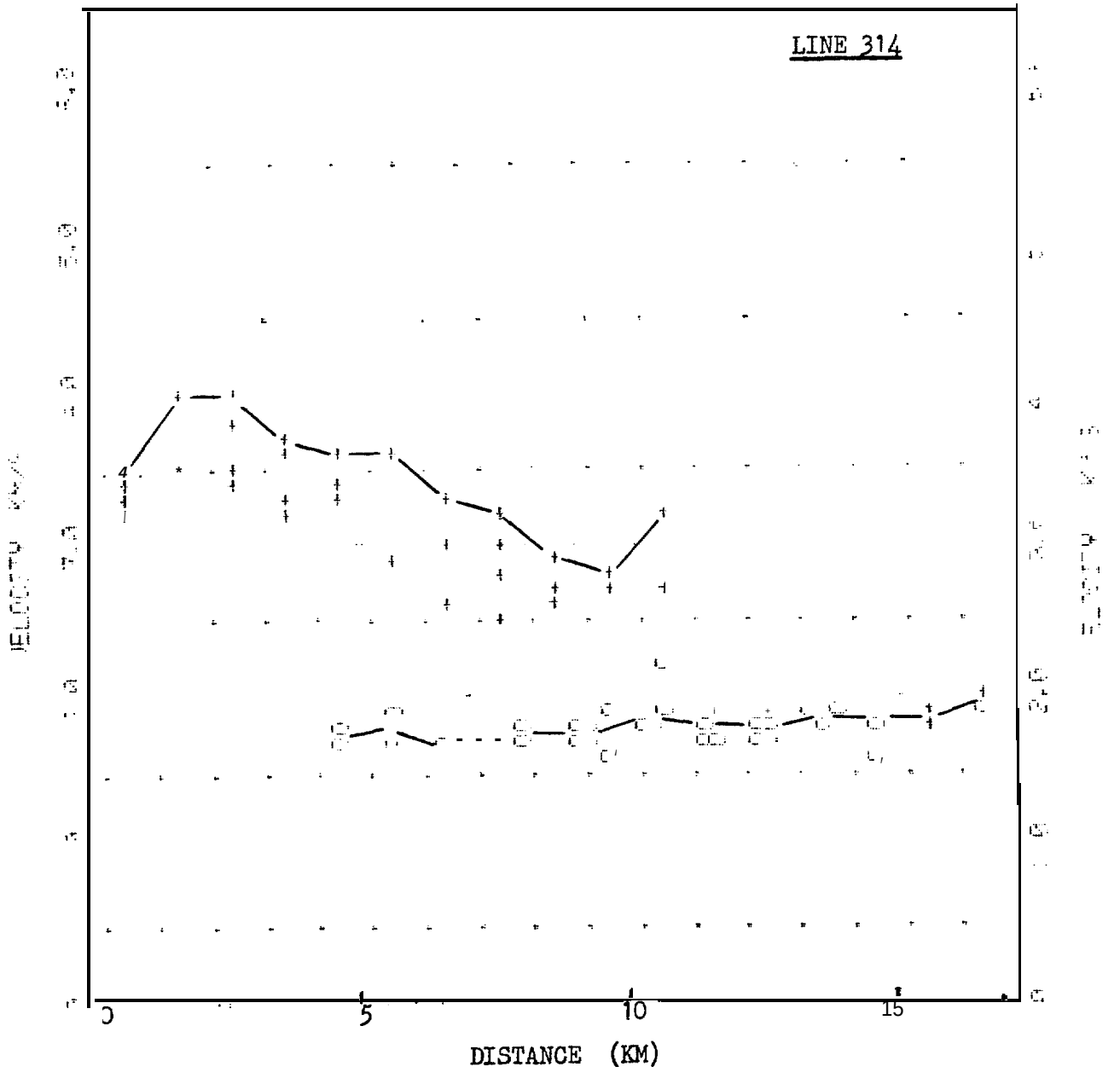
LINE 314
0
5
10
15
DISTANCE (KM)

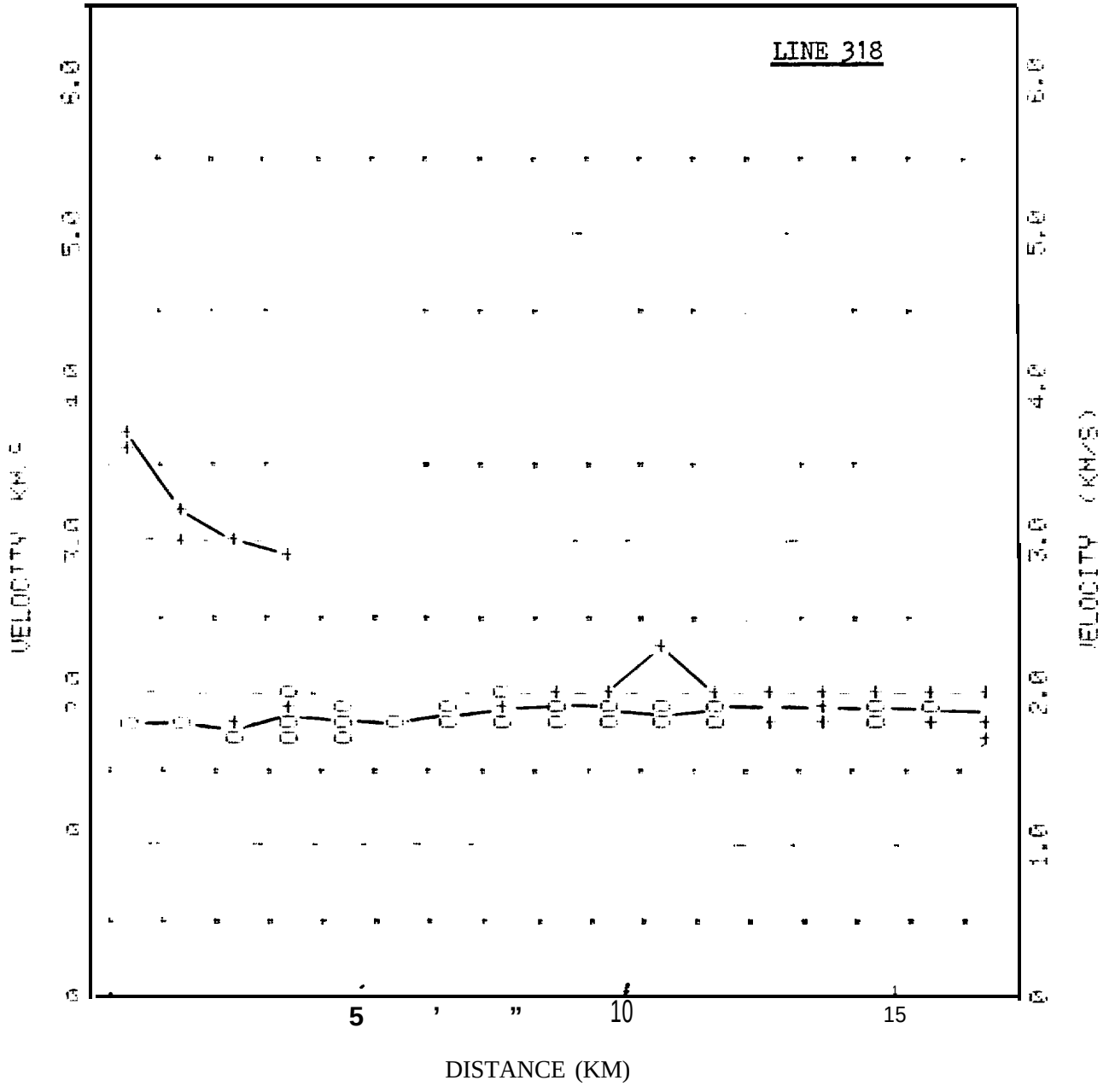
LINE 318
VELOCITY KM/S
VELOCITY (KM/S)
6.0
5.0
4.0
3.0
2.0
1.0
0
5
10
15
DISTANCE (KM)

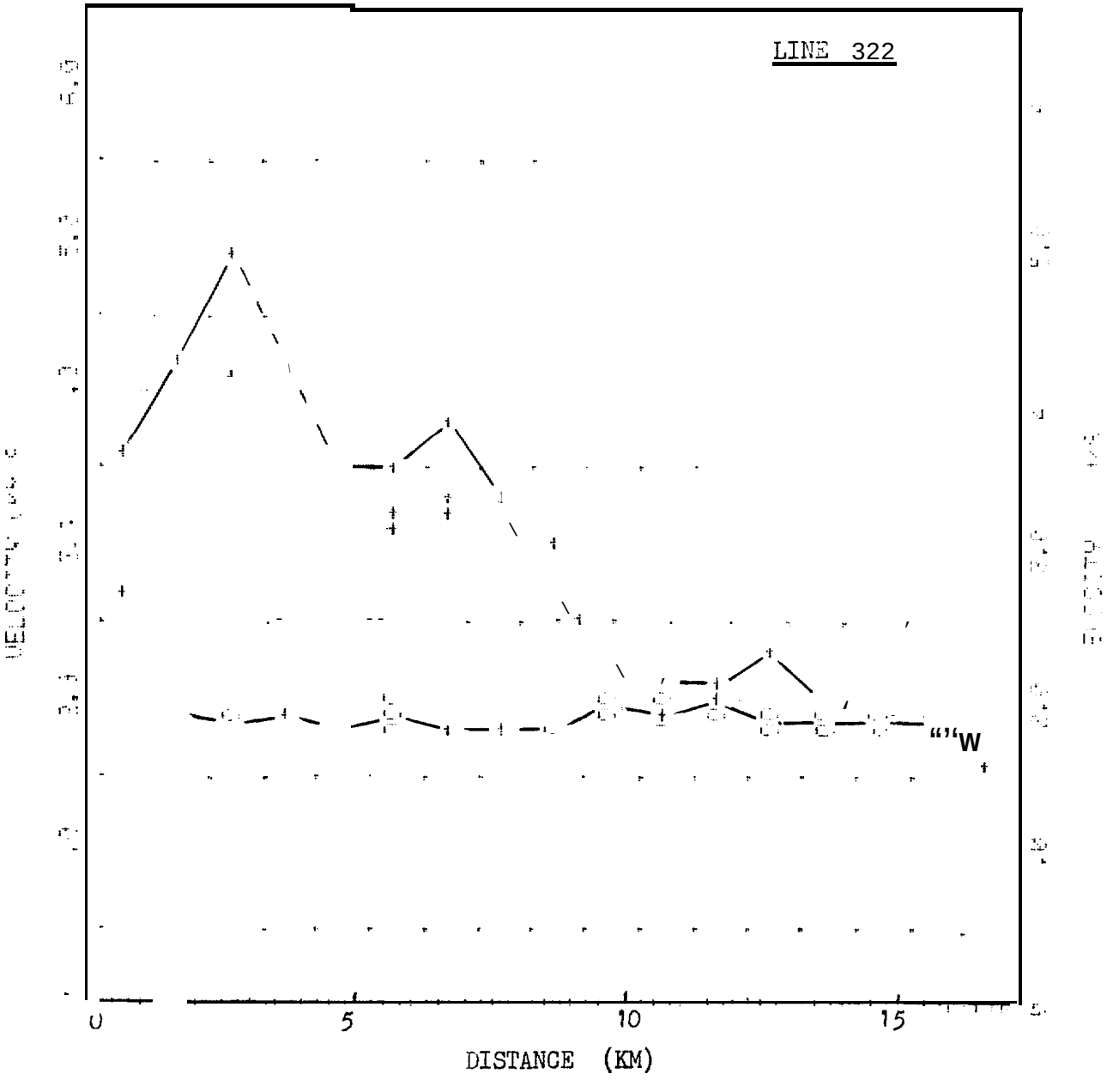
LINE 322
0
5
10
15
DISTANCE (KM)

LINE 326
DISTANCE (KM)
0
1
2
20

LINE 328
VELOCITY (KM/S)
1.0
2.0
3.0
4.0
5.0
6.0
DISTANCE (KM)
0
5
10
20
25
30

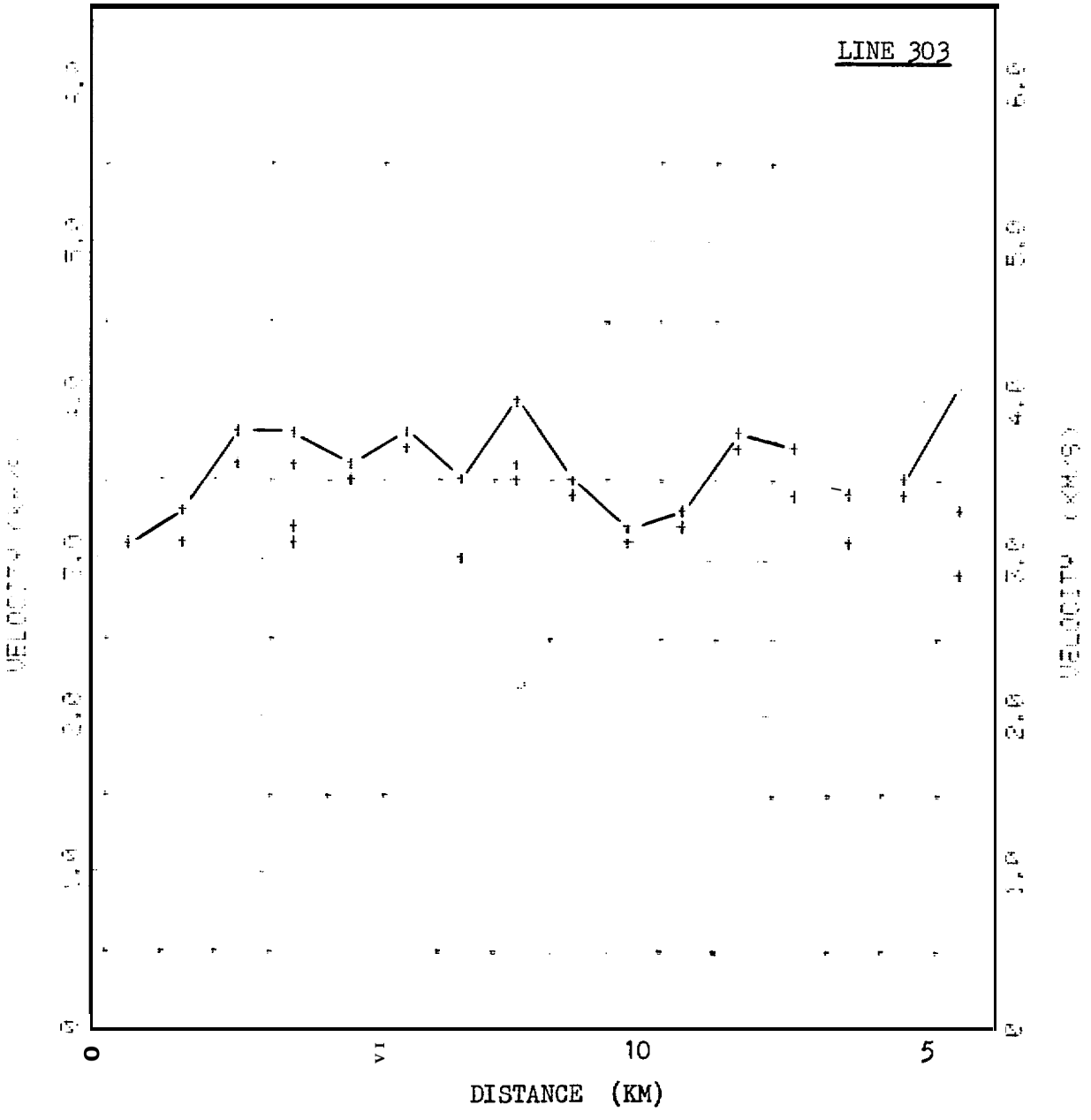
LINE 303
0
10
5
DISTANCE (KM)

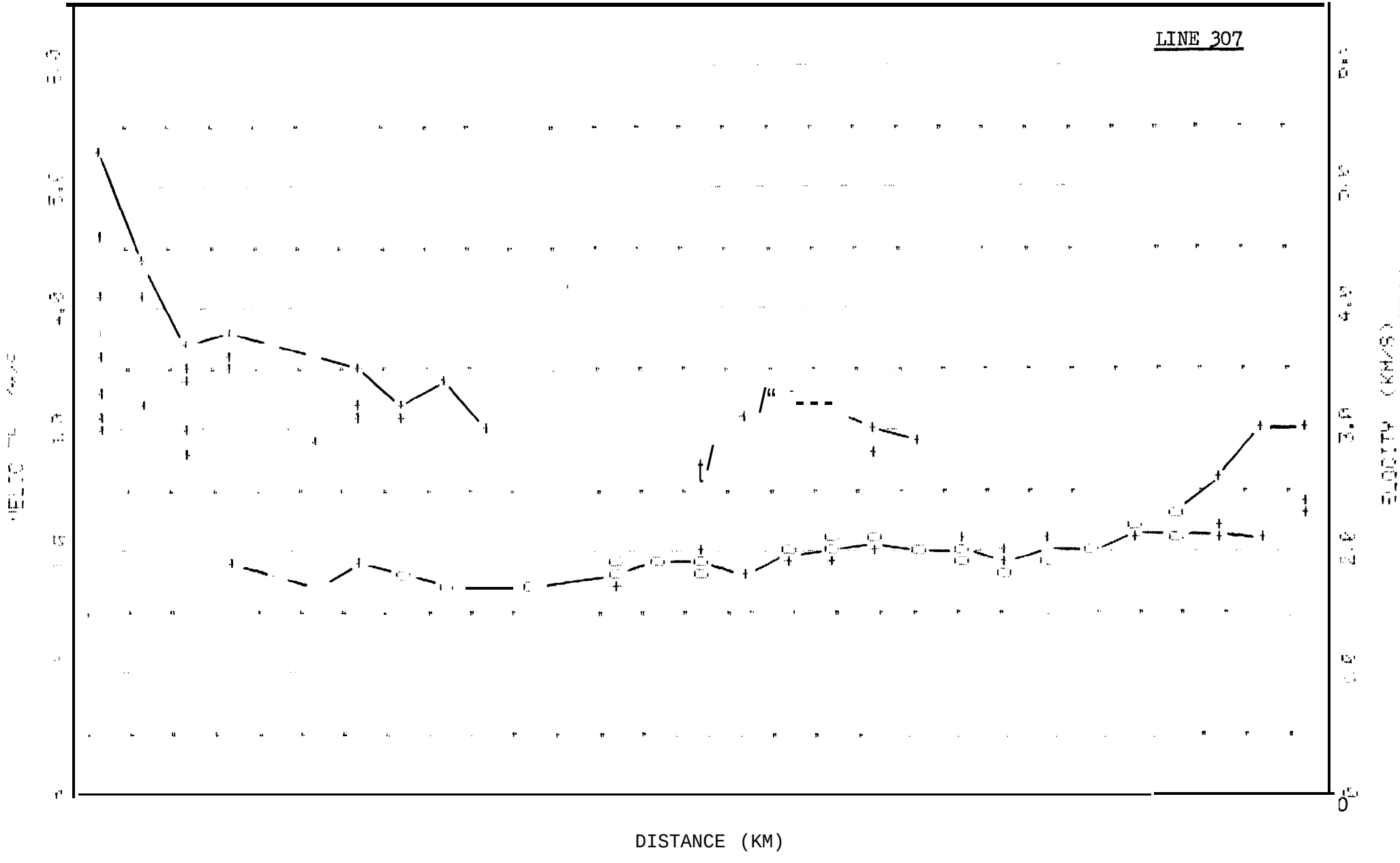
LINE 307
DISTANCE (KM)

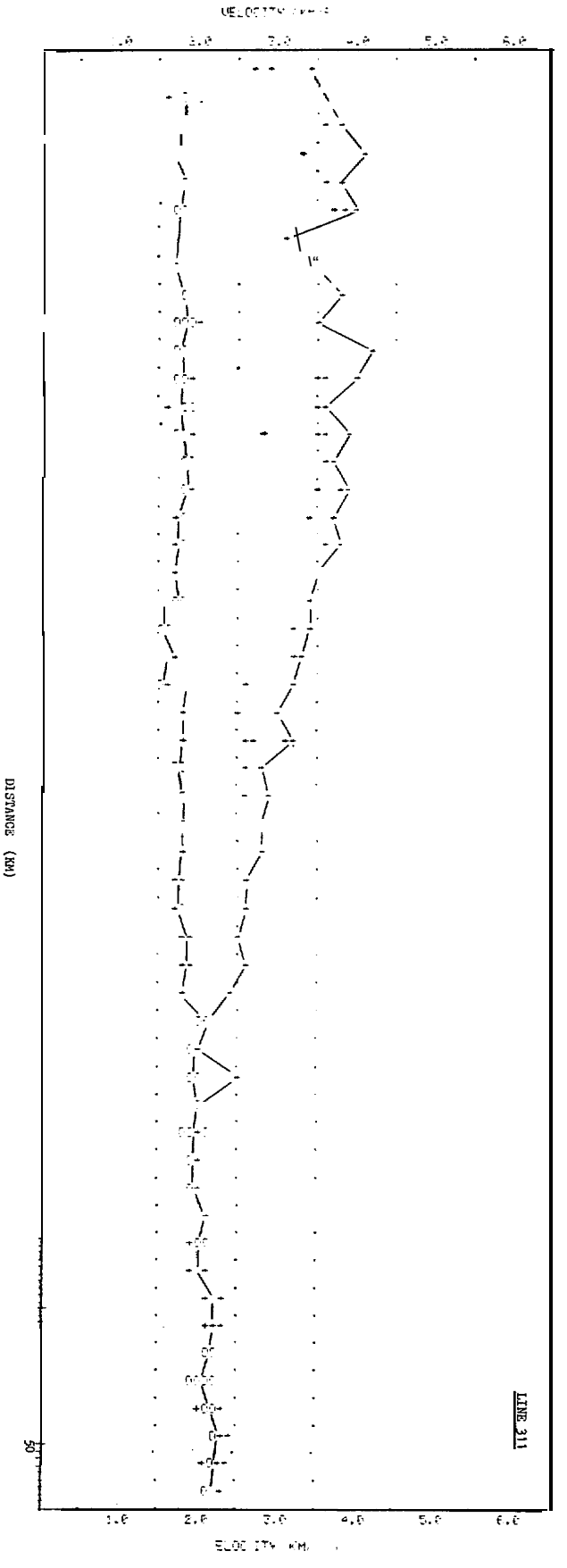
1.0
2.0
3.0
4.0
5.0
6.0
DISTANCE (KM)
50
LINE 211

APPENDIX C: SEISMIC CROSS SECTIONS

The following depth profiles show a northeast dip of 1-3% for the refracting horizon. Three lines (D26, D30 and D31) have the high velocity material rising to meet the shoreline. Refraction multiples are found on a number of profiles. Vertical expression is 28:1.

The following legend applies to the profiles:

+ Refraction depth (velocity < 2.(I km/s)

* Refraction depth (velocity $\geq$ 2.0 km/s)

O Reflection depth.

The location of the lines can be found in Figure 1.

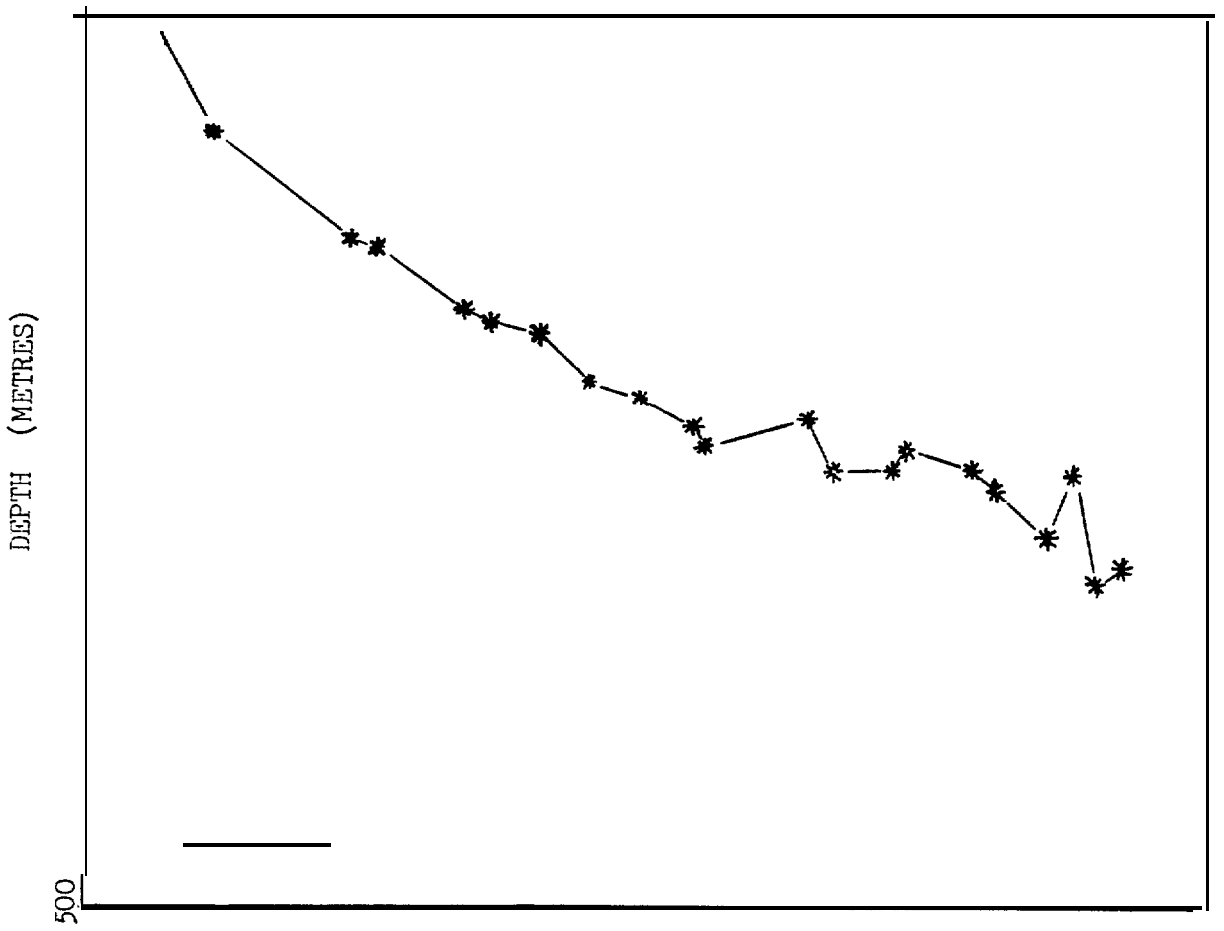
DEPTH (METRES)
500

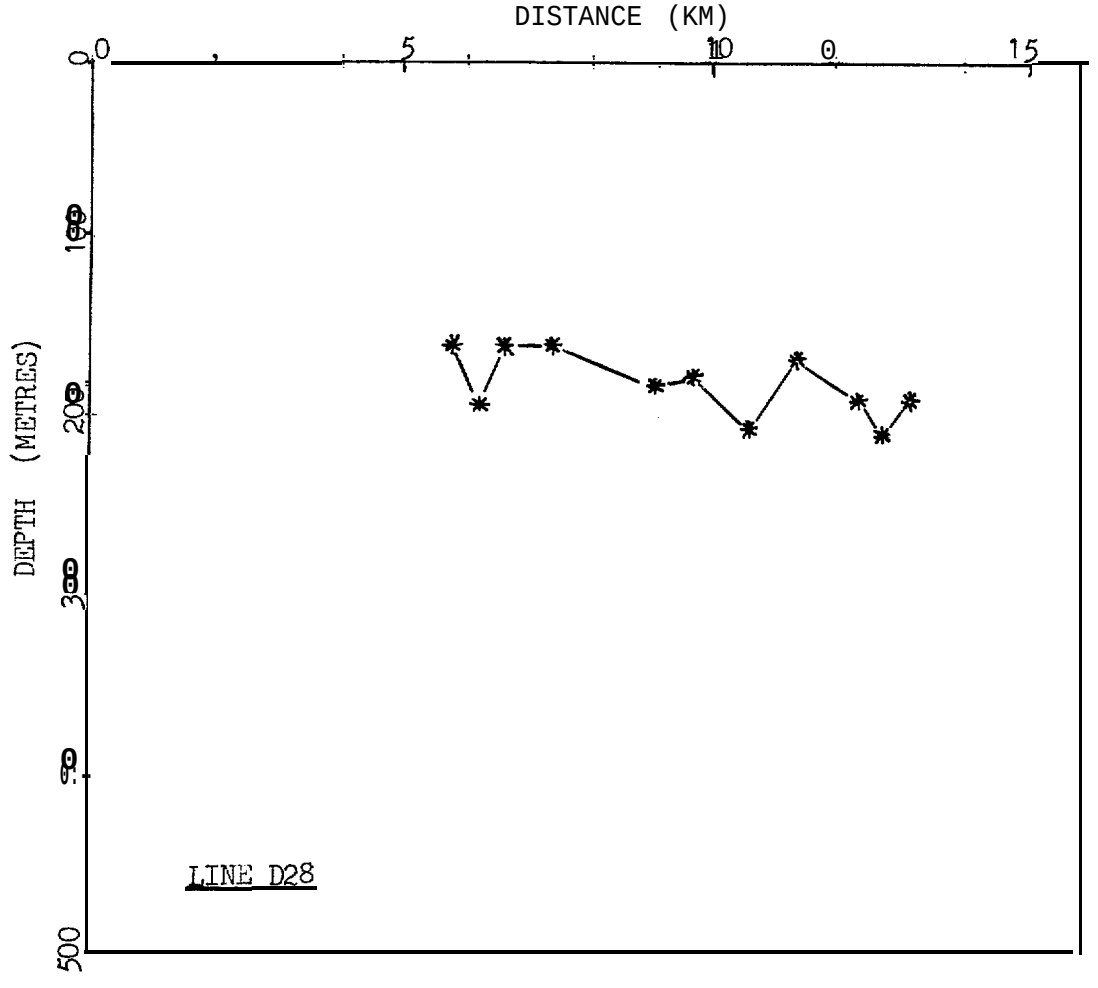
DISTANCE (KM)
0
5
10
15
DEPTH (METRES)
100
200
300
500
LINE D28

DISTANCE (KM)
5
10
15
20
DEPTH (METRES)
LINE D29

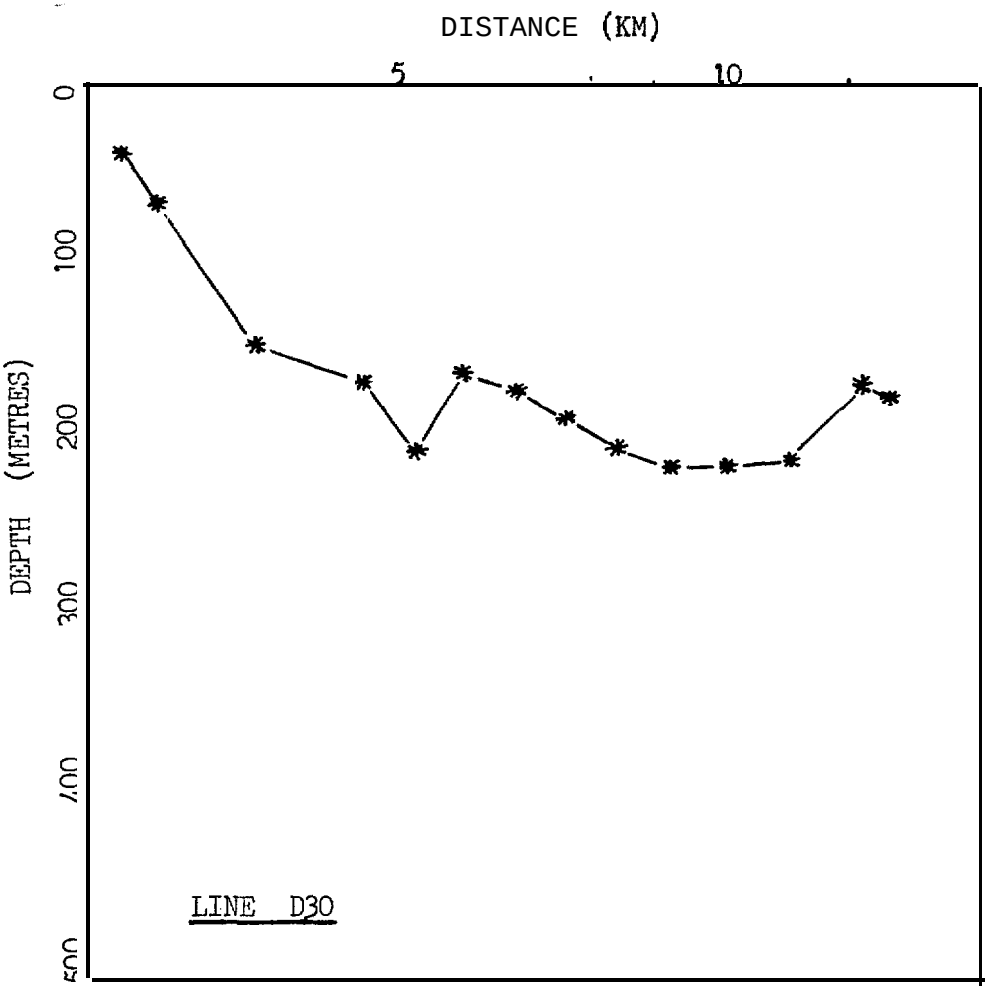
DISTANCE (KM)
5
10
0
100
200
300
DEPTH (METRES)
LINE D30

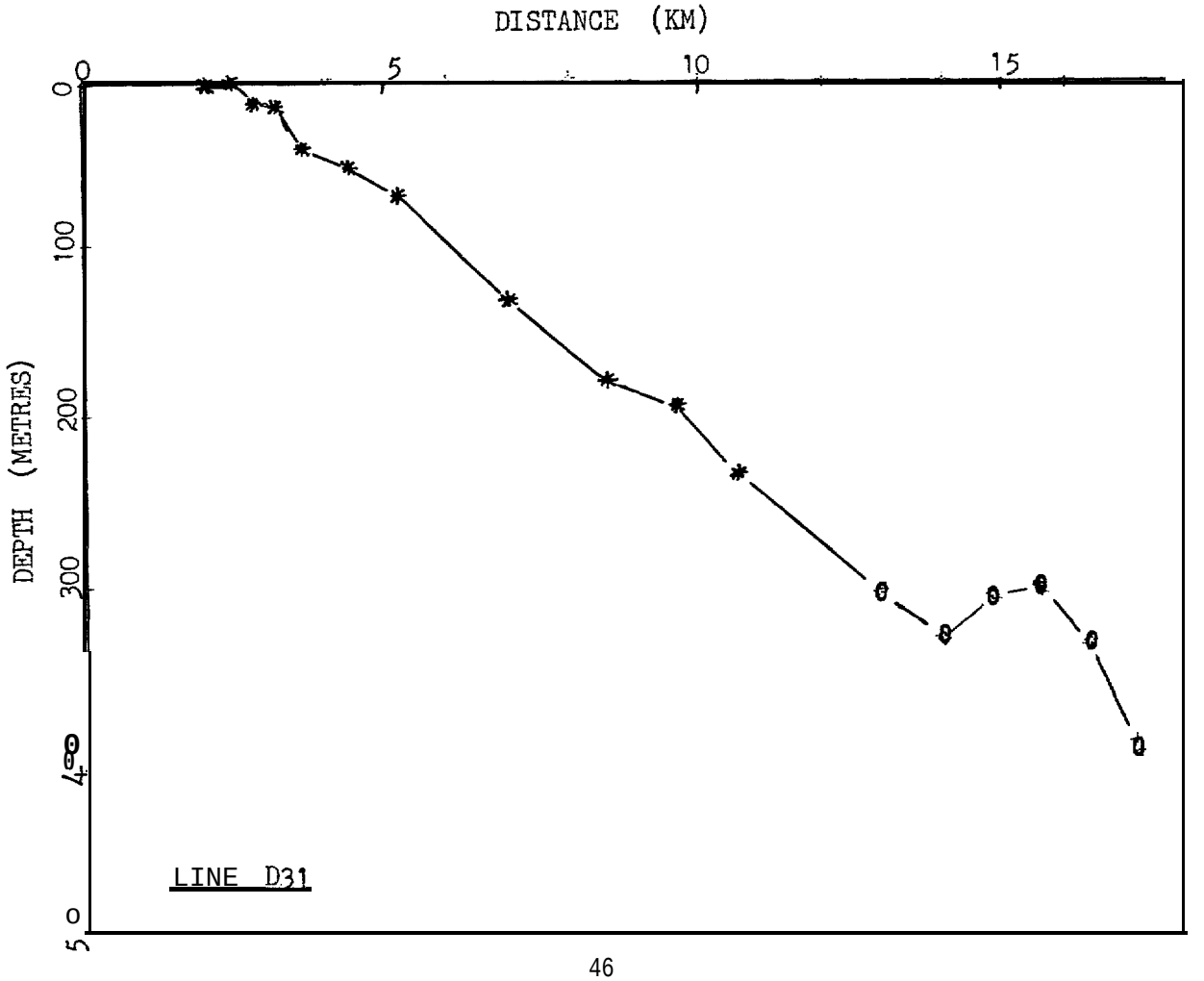
DISTANCE (KM)
0
5
10
15
0
100
200
300
DEPTH (METRES)
LINE D31

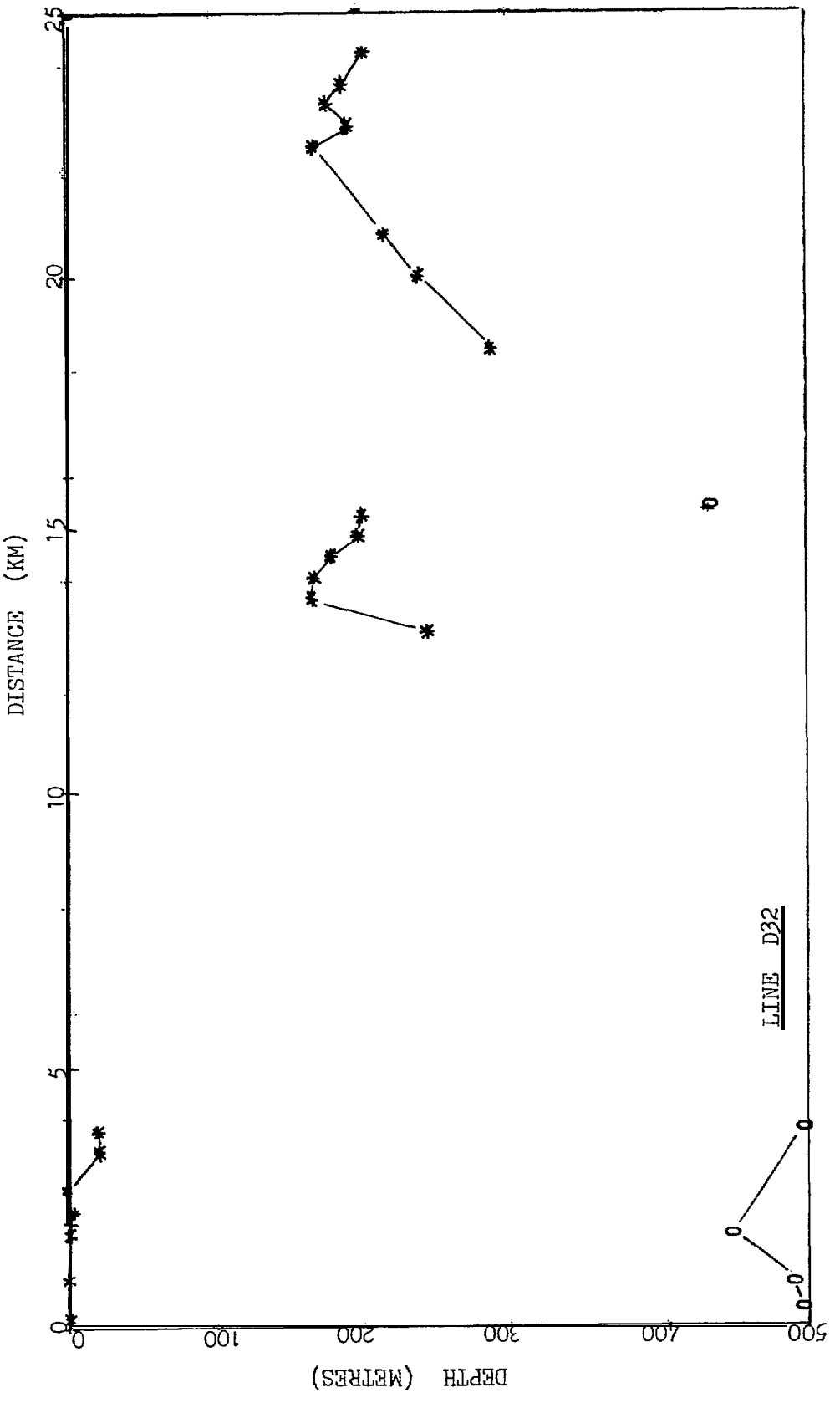
LINE D32
DISTANCE (KM)
0
5
10
15
20
25
DEPTH (METRES)
0
100
200
300
400
500

DISTANCE (KM)
0
10
15
20
25
30
0
100
200
300
400
500
DEPTH (METRES)
LINE D33

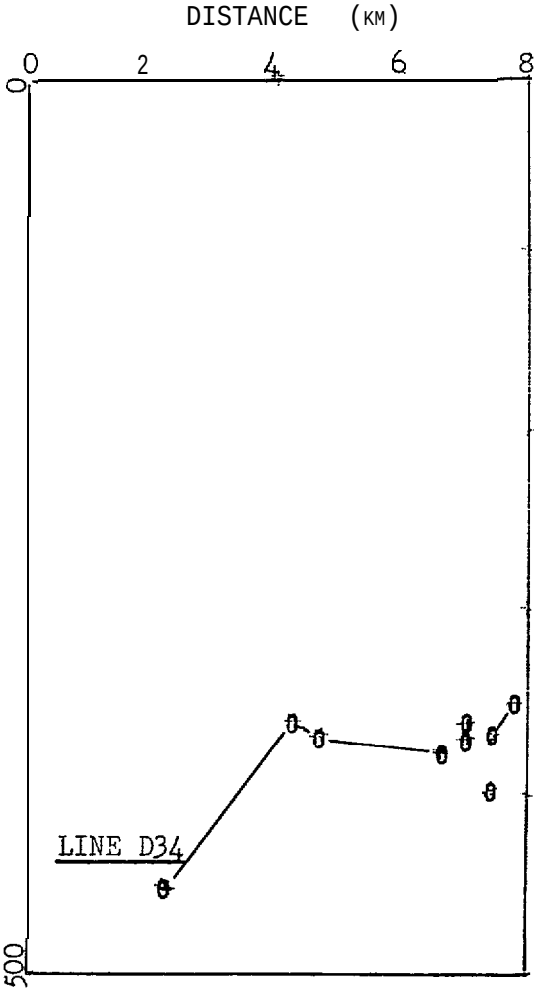
DISTANCE (KM)
0
2
4
6
8
0
500
LINE D34

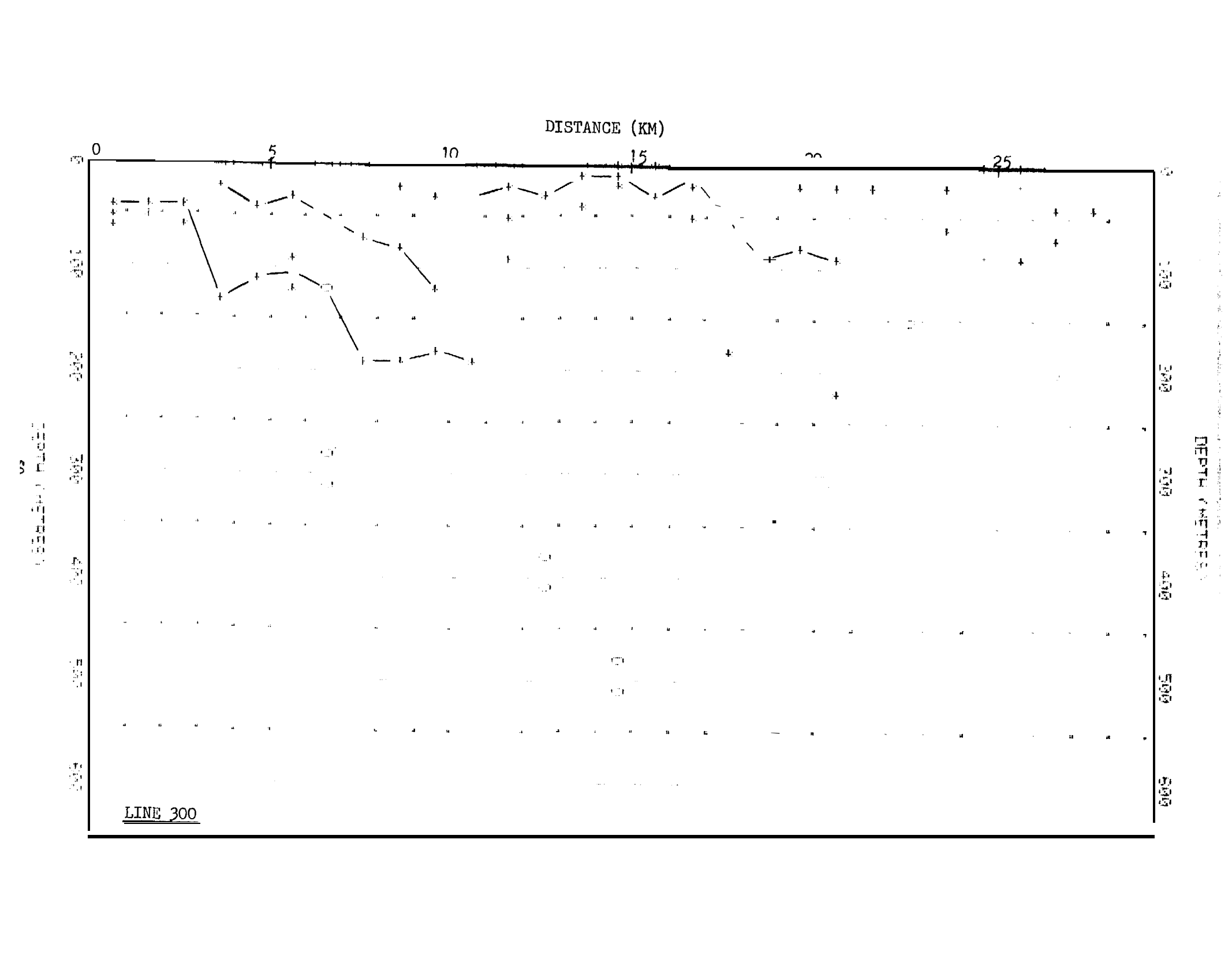
DISTANCE (KM)
0
5
10
15
25
LINE 300

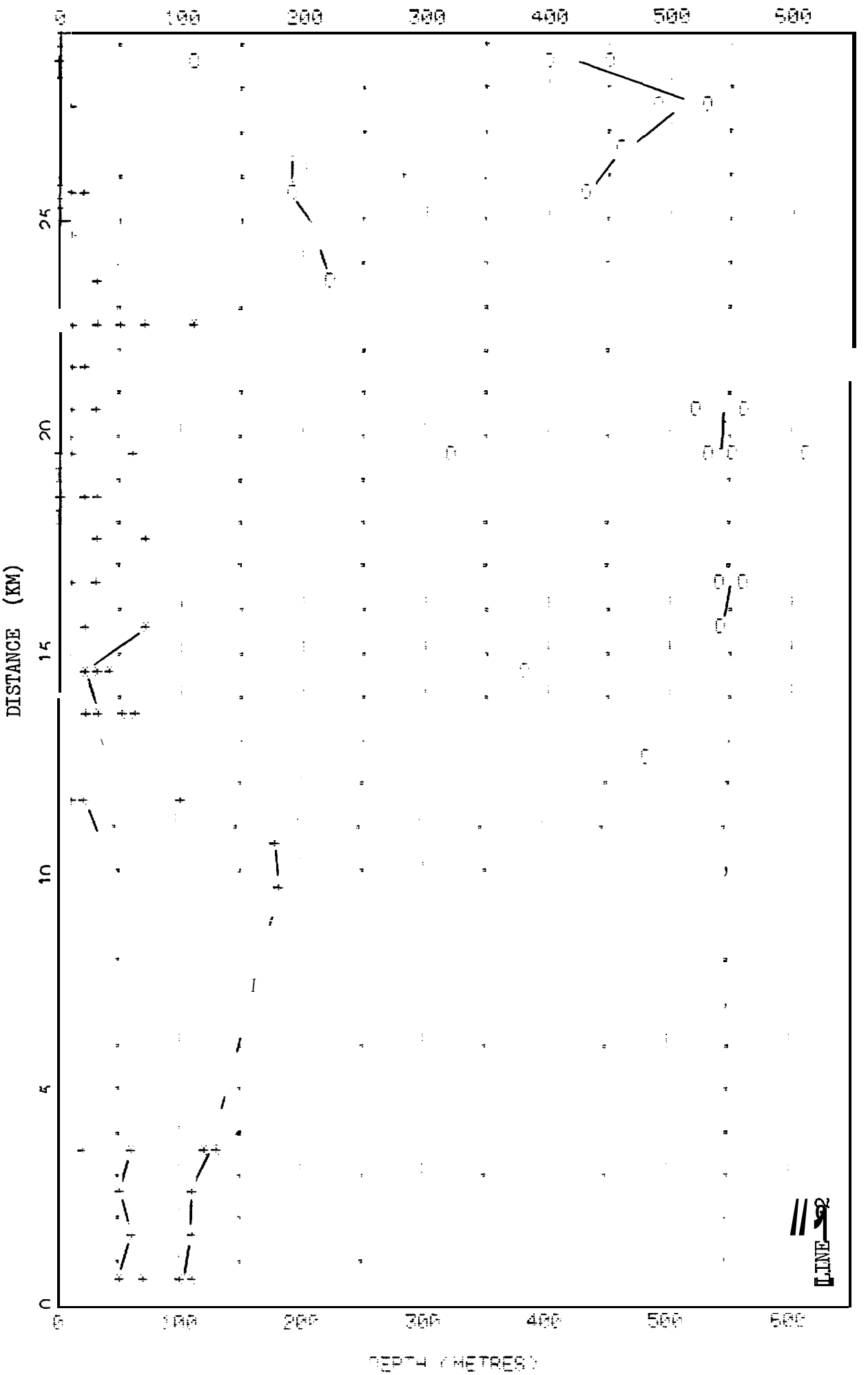
0
100
200
300
400
500
600
25
20
15
10
5
0
DISTANCE (KM)
DEPTH (METRES)
LINE 2

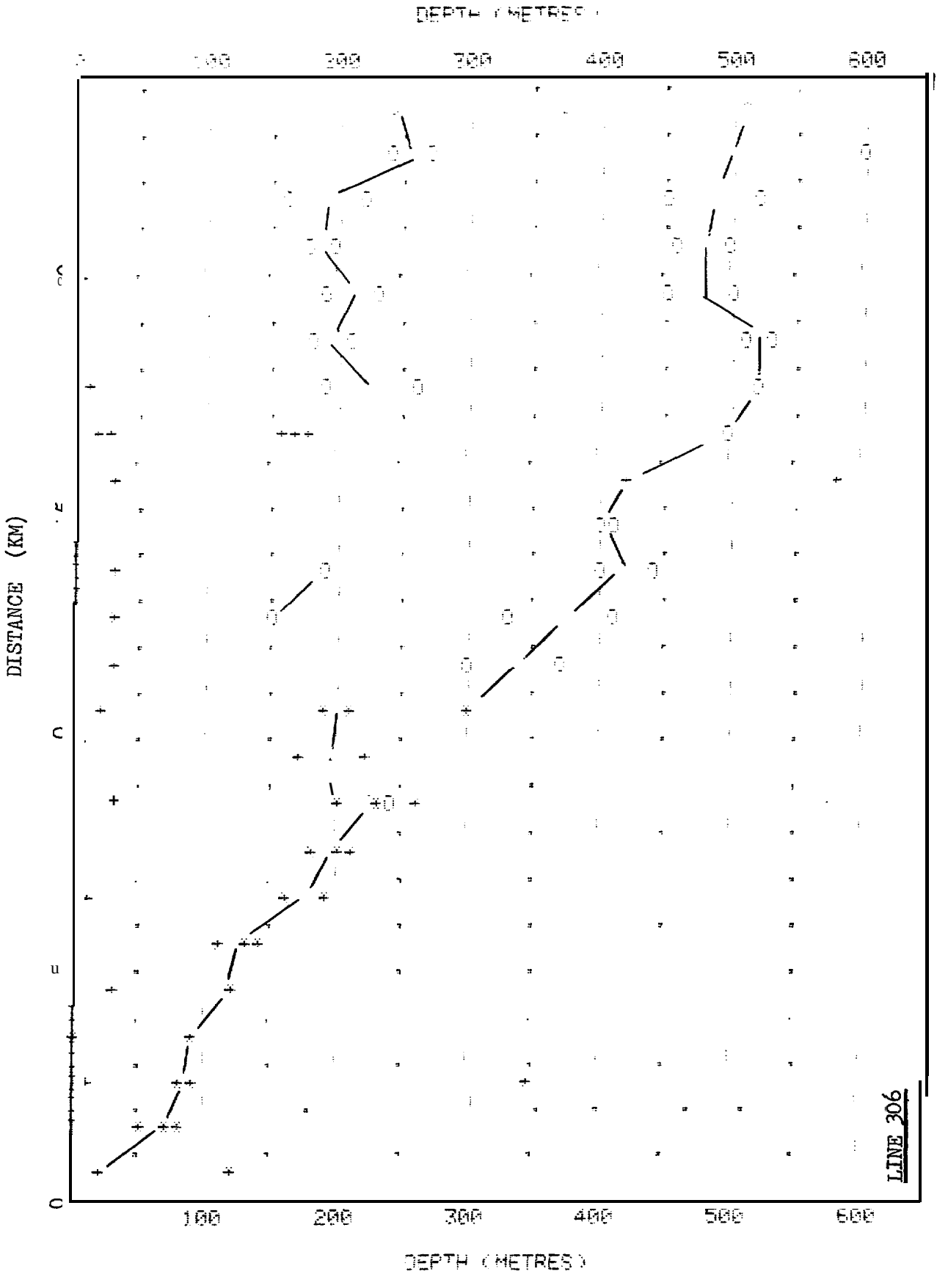
DEPTH (METRES)
100
200
300
400
500
600
DISTANCE (KM)
0
LINE 306
DEPTH (METRES)

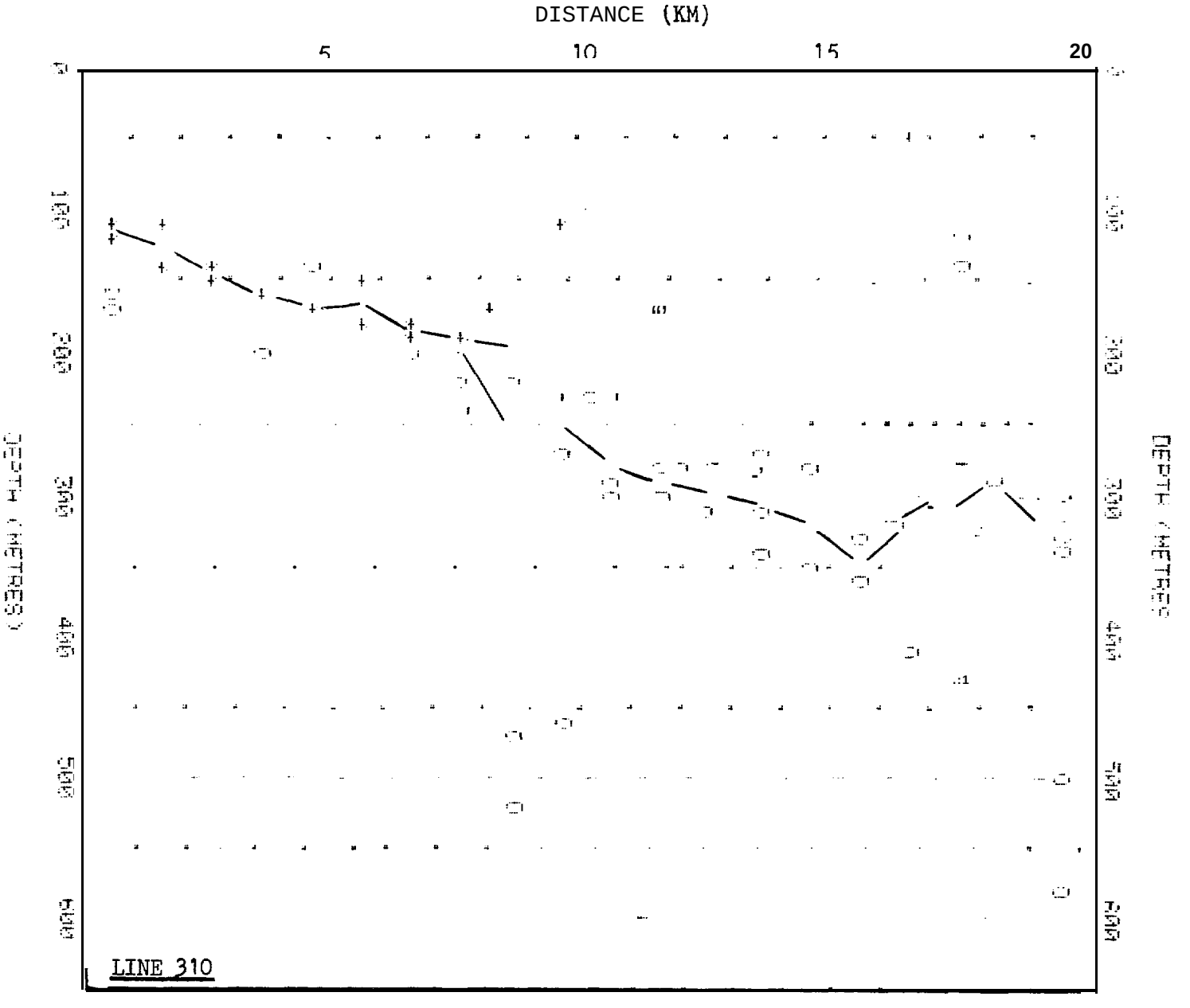
DISTANCE (KM)
5
10
15
20
LINE 310

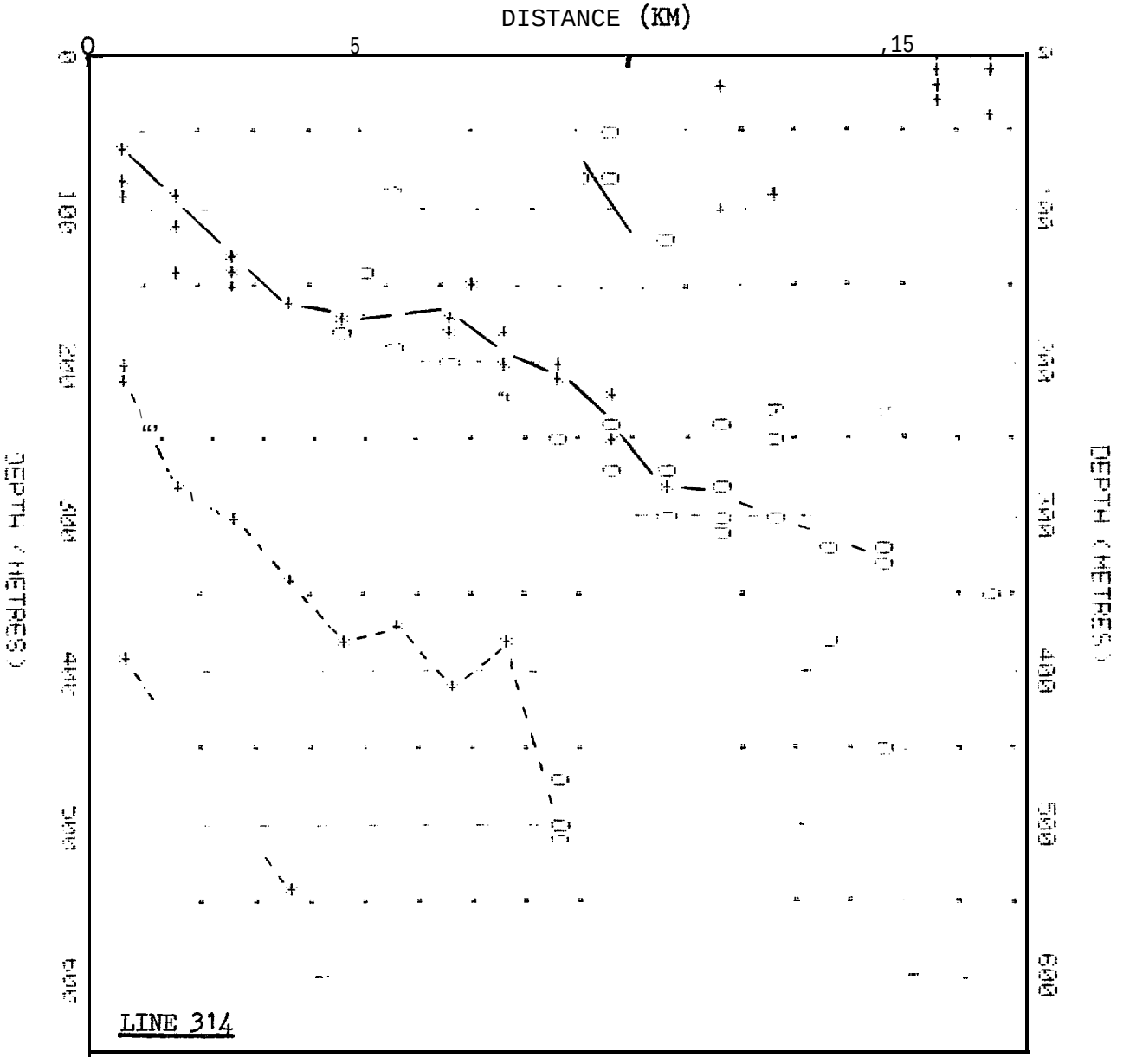
DISTANCE (KM)
0
5
15
DEPTH (METRES)
LINE 314

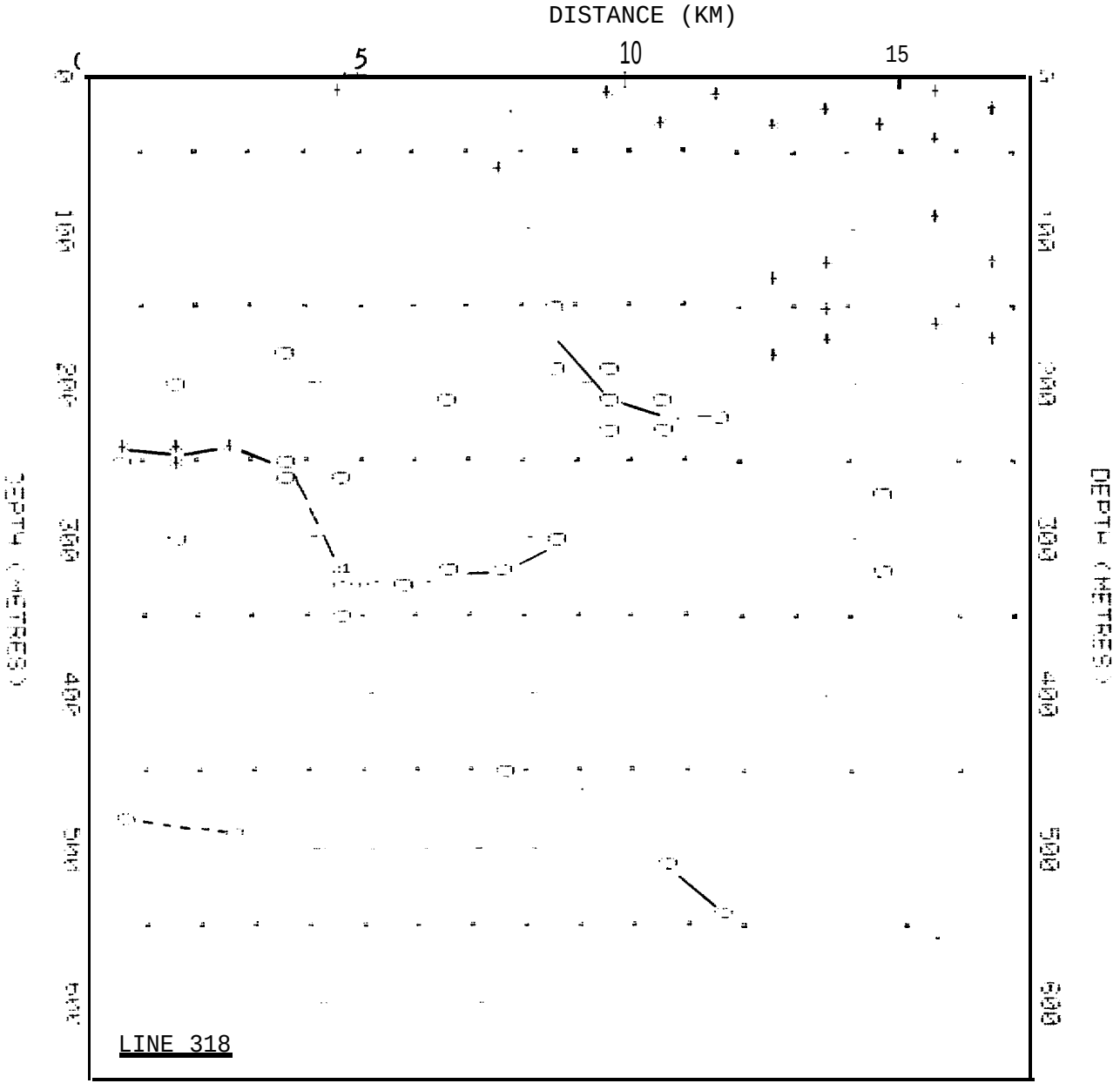
DISTANCE (KM)
5
10
15
LINE 318

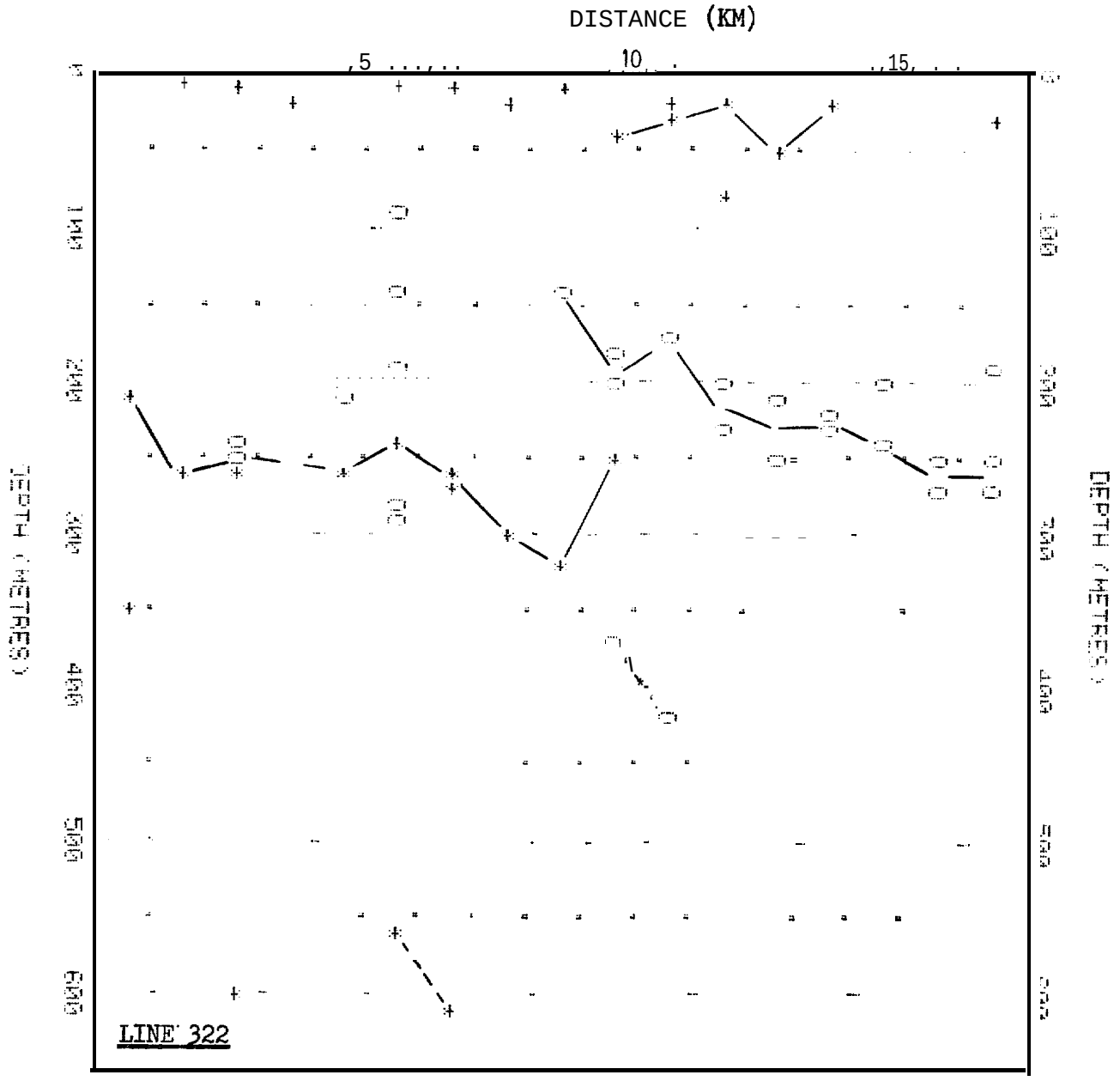
DISTANCE (KM)
5
10
15
DEPTH / METRES
LINE 322

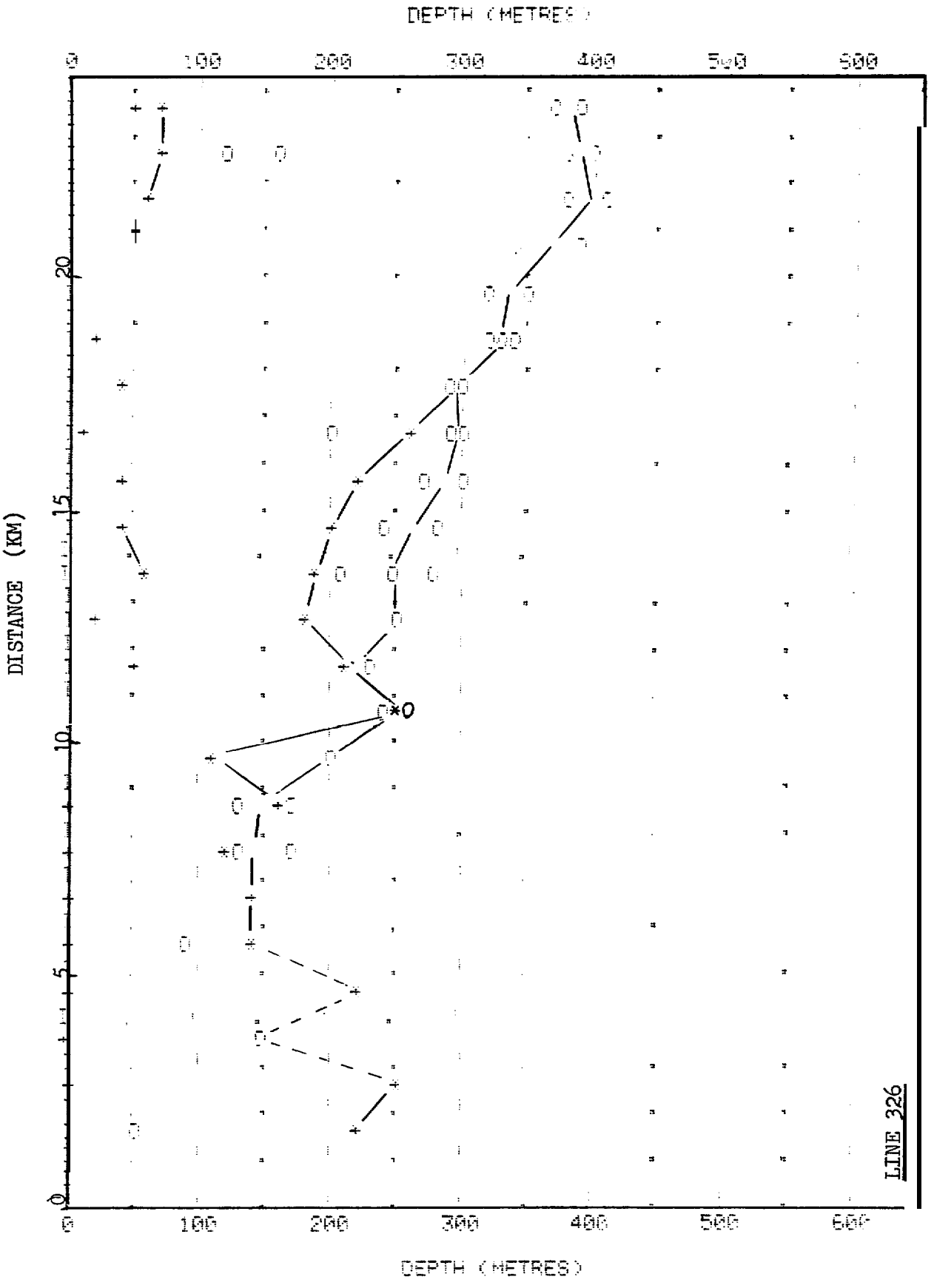
DEPTH (METRES)
0
100
200
300
400
500
DISTANCE (KM)
0
5
10
15
20
LINE 326

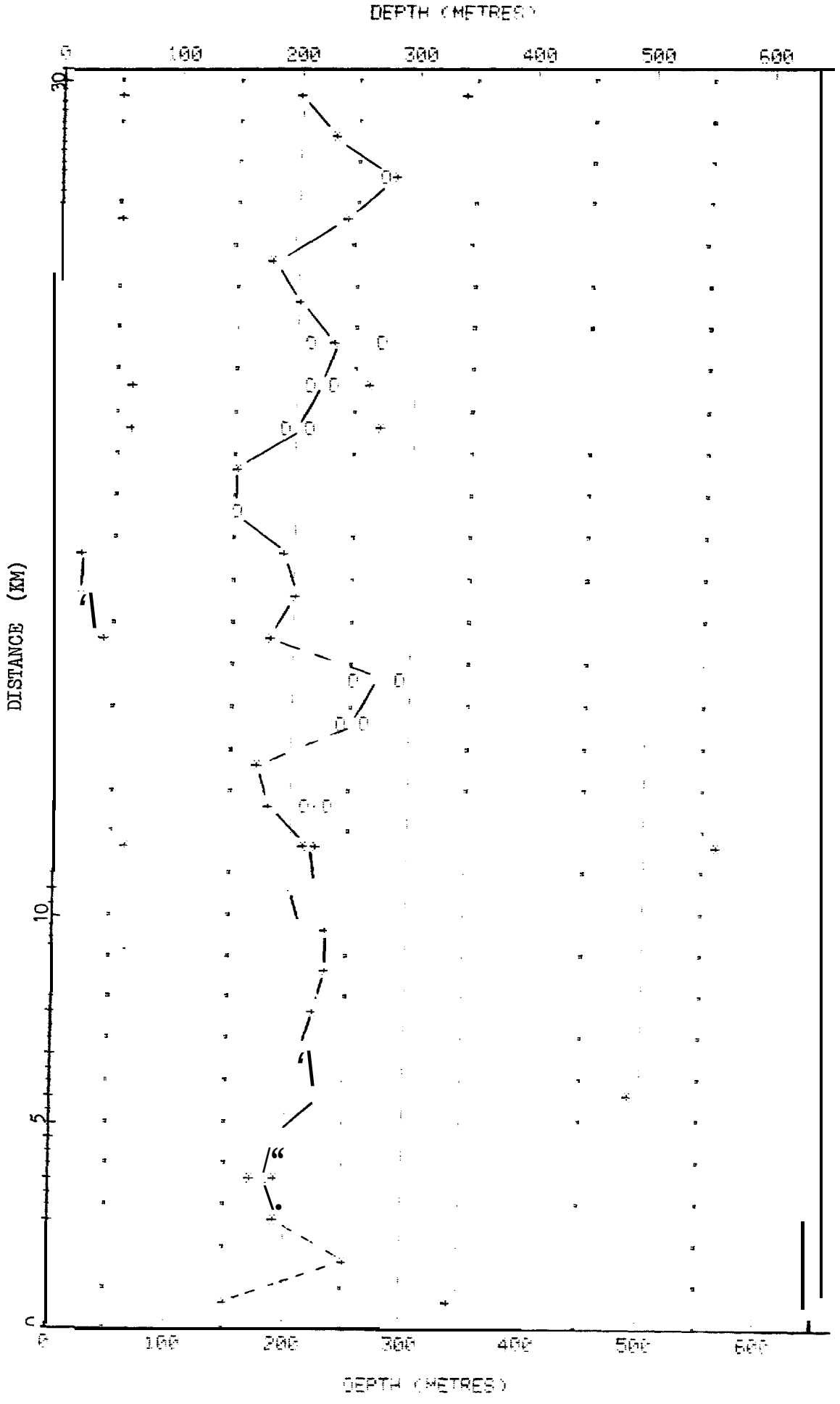
DEPTH (METRES)
0
100
200
300
400
500
600
30
10
5
0
DISTANCE (KM)
DEPTH (METRES)

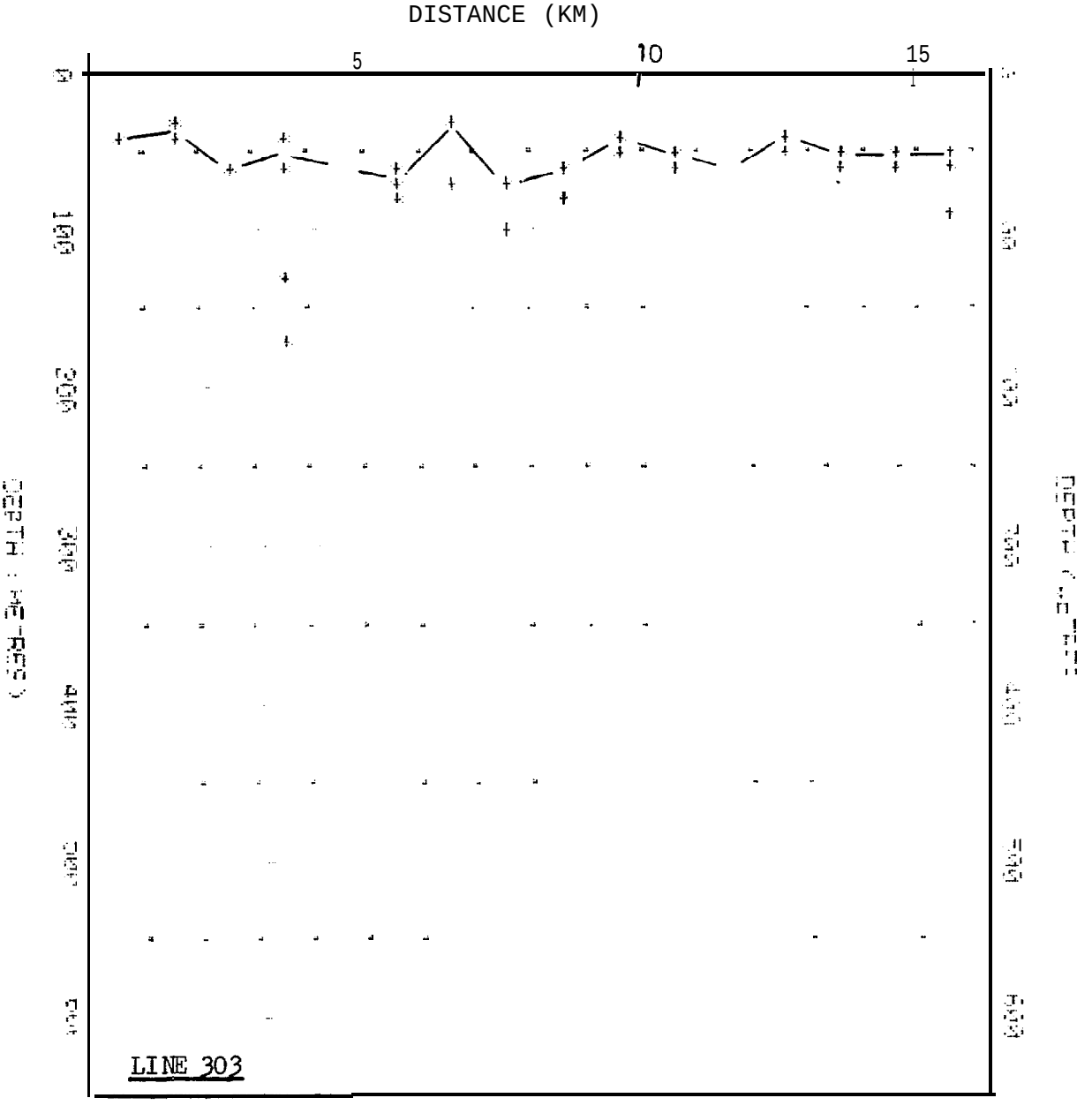
DISTANCE (KM)
5
10
15
LINE 303

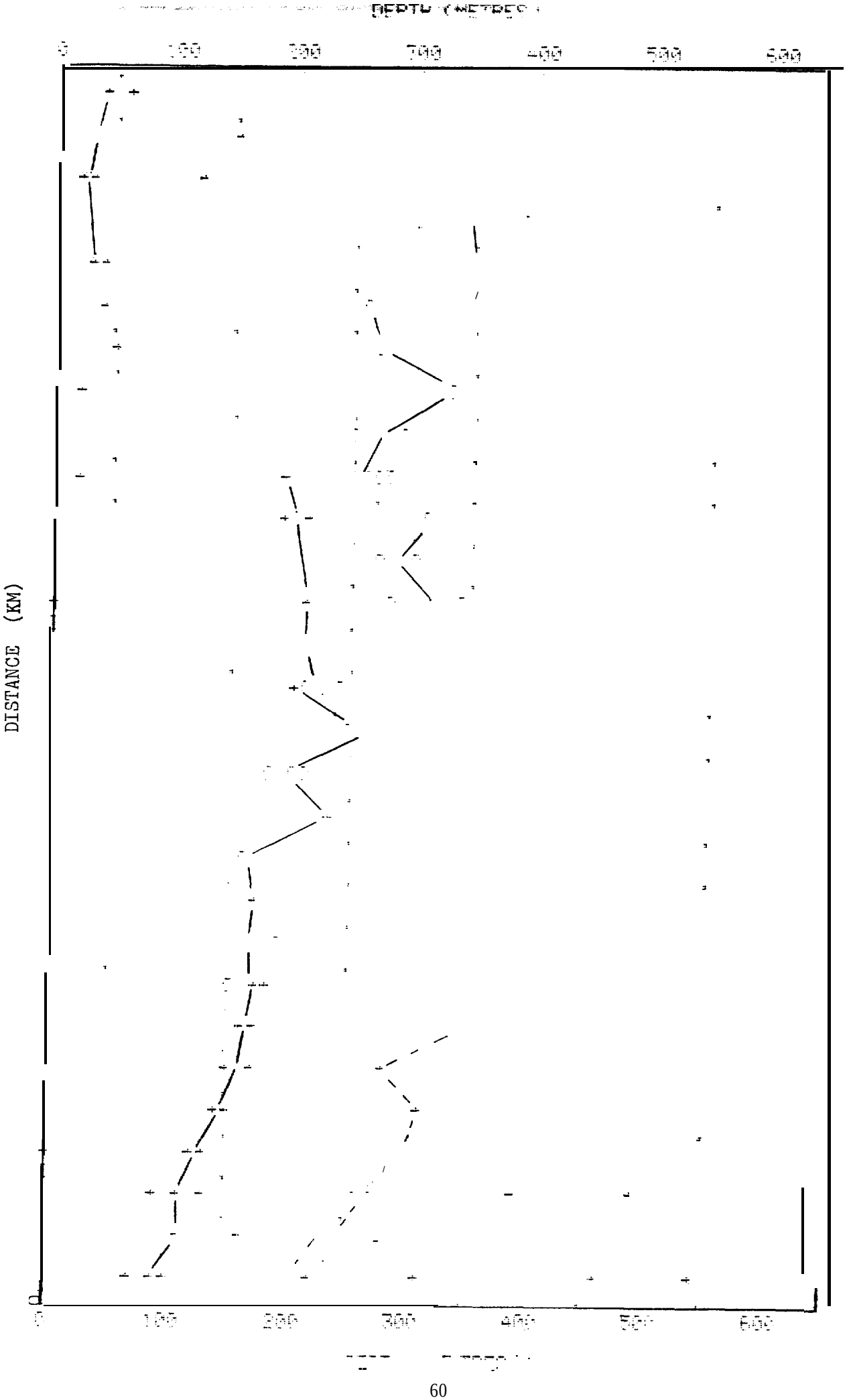
DEPTH (METRES)
0
100
200
300
400
500
600
DISTANCE (KM)
0
100
200
300
400
500
600

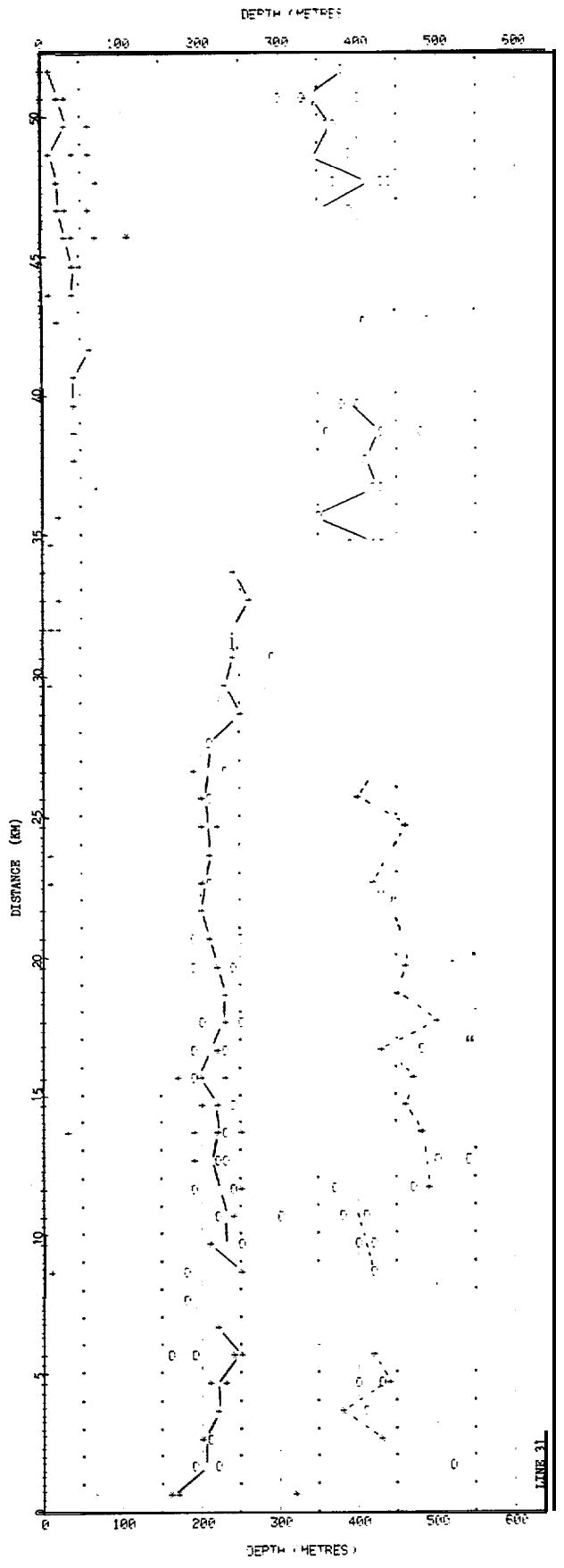
DEPTH (METRES)
0
100
200
300
400
500
600
DISTANCE (KM)
0
5
10
15
20
25
30
35
40
45
50
LINE 31
DEPTH (METRES)

A facsimile catalog card in Library of Congress MARC format is reproduced below.

Neave, K. Gerard
Subsea permafrost in Harrison Bay, Alaska: An interpretation from seismic data / by K. Gerard Neave and Paul V. Sellmann. Hanover, N.H.: U.S. Army Cold Regions Research and Engineering Laboratory; Springfield, Vs.: available from National Technical Information Service, 1982.
iv, 68 p., illus.; 28 cm. (CRREL Report 82-24.)
Prepared for Dept. of Interior, Bureau of Land Management, and Dept. of Commerce, National Oceanic and Atmospheric Administration by Corps of Engineers, U.S. Army Cold Regions Research and Engineering Laboratory.
Bibliography: p. 16.

SEE NEXT CARD

Neave, K. Gerard
Subsea permafrost in Harrison Bay...
1982 (card 2)

1. Alaska-Seismology. 2. Beaufort Sea-Seismology. 3. Permafrost. 4. Seismic data. 5. Seismic detection. 6. Seismic reflection. 7. Seismic signatures. 8. Seismology. I. Sellmann, Paul V. II. United States. Army. Corps of Engineers. III. Army Cold Regions Research and Engineering Laboratory, Hanover, N.H. IV. Series: CRREL Report 82-24.